Title: Enhancing the SPDE modeling of Spatial Point Processes with INLA, applied to wildfires. Choosing the best mesh for each database.

Dr. Pablo Juan Verdoy

Department of Mathematics, Universitat Jaume I, Campus Riu Sec, 12071 Castellón, Spain

Telephone number: +34 964 728381

e-mail: juan@uji.es

ORCID number: http://orcid.org/0000-0002-2197-7502

Abstract

Wildfires play an important role in shaping landscapes and as a source of CO_2 and particulate matter, and are a typical spatial point process studied in many papers. Modeling the spatial variability of a wildfire could be performed in different ways and an important issue is the computational facilities that the new techniques afford us. The most common approaches have been through point pattern analysis or by Markov random fields. These methods have made it possible to build risk maps, but for many forest managers it is very useful to know the size of the fire as well as its location. In this work, we use Stochastic Partial Differential Equation (SPDE) with Integrated Nested Laplace Approximation (INLA) to model the size of the forest fires observed in the Valencian Community, Spain. But the most important element in this paper is the process that needs to be carried out prior to simulating and analyzing the different point patterns, namely, the choice of the most suitable mesh for the database. We describe and take advantage of the Bayesian methodology by including INLA and SPDE in the modeling process in all the scenarios.

Keywords: Bayesian Inference, INLA, Mesh, Spatial Point Process, SPDE.

1. Introduction

Modeling the spatial incidence of wildfires and the fire size is necessary to understand how global warming and climate change may affect the landscape in the coming years, and to determine what factors are related to spatial incidence and the size of the area burned (e.g., Díaz-Avalos et al., 2001, and Díaz-Avalos et al., 2016). Wildfires can be associated with their spatial coordinates and the corresponding covariates, and this association makes it easier to represent them as a realization of a spatial stochastic process. Thus, even though methods such as Markov Random Fields may also be useful to respond to some scientific questions of interest, spatial point processes are the most appealing analytical tool to analyze the spatial and spatio-temporal distribution of forest fires (Mandallaz and Ye, 1997; Xu and Schoenberg, 2011). Spatial point process theory is a rich subject that provides the mathematical fundamentals required to sustain methods that are useful to analyze phenomena with a spatial variation and make it possible to screen out the general factors that are related to such spatial variation. For a good introduction to spatial point processes, see Möller and Waagepetersen (2006).

Previous studies have dealt with the problem of producing risk maps or of calculating the probability of a wildfire starting at some location inside a study area *D* using statistical methods (e.g., Serra et al., 2014 a, b; Barros and Pereira, 2014). Despite their usefulness, most of the studies have not considered the burned area caused by each wildfire in the same way as in this paper. Statistical methods used to produce wildfire

risk maps have included Markov Random Fields (Díaz-Avalos et al., 2001) and spatial point processes (Juan et al., 2012; Møller and Díaz-Avalos, 2010; Serra et al., 2014 a, b). All these approaches have included the effect of spatial covariates.

Nevertheless, the previous points in the work are the process of simulating, analyzing and modeling the three real patterns: regular, inhibition and cluster. We fitted several models, starting with models that include two simulated covariates. All the models have been compared with the use of Deviance Information Criterion (DIC) and the Watanabe-Akaike information criterion (WAIC) (Spiegelhalter et al., 2002; Watanabe, 2010).

Moreover, the most important objective of this work is to show the benefits of using Stochastic Partial Differential Equation (SPDE) with Integrated Nested Laplace Approximation (INLA) for spatial data (Ehlers and Zevallos, 2015; Lindgren et al., 2011; Martins, et al. 2013; Neyens et al., 2018; R-INLA, 2015; Rue et al., 2009; Ruiz-Cárdenas et al., 2012). Previous studies (Taylor and Diggle, 2013) have described the difficulty of working with INLA for specific parameters, i.e., spatial parameters, but this problem could be solved with the use of SPDE in the majority of scenarios.

Previously, however, it is necessary to introduce the methodology, the simulation, and the usefulness of this methodology. This will be done step by step. Some previous papers (e.g., Díaz-Avalos et al., 2016) have identified the main problem of using this methodology as the choice of mesh, but this was only a small step. In this paper we present the procedure for the real process of analyzing the different spatial point processes more accurately, as previously defined.

Nowadays, the problem is to choose the perfect mesh formed with the SPDE of each pattern in a spatial point process, which is the main objective in this paper. Thus, it will be a valuable aid for researchers who are faced with the question: which is the correct mesh for my case?

The rest of the paper is organized as follows: Section 2, Methods, gives all the details needed to clarify the Bayesian methodology used and Spatial Point Process; Section 3, the Simulation study, is followed by the models for the simulated data in Section 4. Section 5 describes and discusses the results and the interpretation of applied wildfire data. We finish with Discussion and conclusions in Section 6. To end, the code used is presented in Appendix A and other graphical results are shown in Appendix B.

2. Methods

Spatial Point Processes

A spatial point process is a stochastic process in which we observe the locations of some events of interest within a bounded region D (Bivand et al. 2007). Spatial point process models are useful tools to model irregularly scattered point patterns that are frequently encountered in all kinds of studies. Except in the simplest cases (Poisson processes), the points or individuals (wildfires) of a spatial pattern will be mutually stochastically dependent. The simplest of all possible models is the constant intensity Poisson process, frequently referred to as the model of 'complete spatial randomness' (CSR) (Juan et al., 2012).

The next step is to decide whether the spatial point process is declared regular, cluster or inhibition, but this is not the ultimate question of this paper. This issue has been defined in many papers (e.g., Juan et al. 2012) and here it is assumed that all the possibilities proposed in the spatial point process exist. Modeling and inference for spatial point processes is an issue that has been investigated broadly over the last few years. The wide range of fields of application has been the main engine driving such increased interest. Spatial Poisson processes play an important role in both statistical theory (Daley and Vere-Jones 2003) and applications (Diggle 2003). A large number of papers have discussed inference for spatial point patterns, but mostly in relation to testing the CSR hypothesis (Cressie 1993; Diggle 2003). However, in many applications, modeling issues are related to detecting patterns and interactions between points in the pattern (Baddeley and van Lieshout 1995), although this is not the most important item addressed in this paper, but instead just a previous step.

Integrated Nested Laplace Approximation

This work also offers the possibility of studying Spatial Point Processes in another way, by using INLA. The data can be idealized as realizations of a stochastic process indexed by:

$$Y(\cdot) \equiv \left\{ y(\cdot) \in R \right\}$$

where $y(\cdot)$ is a subset of R.

The advantages of using INLA over other methods, such as basic statistical methods or more complex ones (like Markov Chain Monte Carlo (MCMC) (Tsanas and Xifara (2012)), are the following:

   • It works with reasonable computational times, thereby allowing the user to work with complex models quickly and efficiently.
   • It allows for the integration of as many covariates as desired, and also the incorporation of new covariates in the model in later steps.
   • It allows the level of significance of covariates to be analyzed.
   • It does not require working with normal distributions exclusively, due to the fact that it is based on Bayesian inference.

The data can be presented by a collection of observations $y = \left\{ y_1, ..., y_n \right\}$ (Blangiardo et al., 2013; Cameletti et al., 2013). A temporal correlation structure is a complicated mathematical entity and its practical estimation is very difficult if the covariates are included (Vlad et al., 2015). In statistical analysis, to estimate a general model it is useful to model the mean for the unit using an additive linear predictor, defined on a suitable scale:

$$\eta_i = \beta_0 + \sum_{m=1}^{M} \beta_m z_{mi} + \sum_{l=1}^{L} f_l\left(v_{li}\right)$$

where β_0 is a scalar, which represents the intercept, $\beta = \left(\beta_1, ..., \beta_M\right)$ are the coefficients of the linear effects of the covariates $z = \left(z_1, ..., z_M\right)$ on the response, and $f = \left\{ f_1(.), ... f_L(.) \right\}$ is a collection of functions defined in terms of a set of covariates $v = v(v_1, ..., v_L)$. The first step in defining the structure of the data $y = \left\{ y_1, ..., y_n \right\}$. A very general approach consists in specifying a distribution for y_1 characterized by a parameter ϕ_i (usually the mean $E(y_i)$) defined as a function of a structured additive predictor η_i through a link function $g(.)$ such that $g(\phi_i) = \eta_i$. The additive linear predictor η_i is defined as follows (Blangiardo and Camaletti, 2015):

$$\eta_i = \beta_0 + \sum_i \beta_1 X_i$$

where β_1 represents the coefficient that quantifies the effect of the covariates in the response x_i. This statistical analysis can be carried out with the freeware statistical package R, version 3.4.3 (R Core Team, 2016) and the R-INLA package 2017 (R-INLA 2017).

Different models can be obtained depending on the covariates, marks and pattern considered in each one. Once the battery of competing models has been obtained, the DIC and the WAIC criterium can be obtained for each of them in order to select the best one. The best models would be those with a high level of complexity and a high goodness-of-fit, that is to say, models that show the lowest WAIC and DIC should be chosen (Spiegelhalter et al., 2002; Watanabe, 2010):

$$DIC =' goodness\ of\ fit'+'complexity' = D(\theta) + 2p_D$$

where $D(\theta)$ is the deviance evaluated at the posterior mean of the parameters and p_D denotes the 'effective number of parameters', which measures the complexity of the model (Spiegelhalter et al., 2002). When the model is true, $D(\theta)$ should be approximately equal to the 'effective degrees of freedom', $n - p_D$.

For each model, a covariate X_i is significant in relation to the response variable Y_i if there is no change in the sign between the 0.025 quantile and the 0.975 quantile of the mean of the corresponding β_1. In addition,

the positive sign of the mean of the corresponding β_i implies that the response variable increases when the covariate increases. The higher the mean of β_i is, the more significant the covariate will be.

Stochastic Partial Differential Equation

We consider that the observed data were generated by spatial point processes with covariates or marks. R software (R Core Team, 2016) and the Bayesian estimation methodology, including the basic features of INLA approach and the SPDE (Lindgren et al., 2011; R-INLA, 2015; Rue et al., 2009), were used to fit parametric models of the observed spatial patterns of wildfires, including covariates that will play the role of risk factors showing spatial variability. This approach makes it possible to account for the effects of the risk factors on the spatial distribution of wildfire patterns (Aragó et al., 2016).

A technical difficulty to fit models using continuously indexed Gaussian random fields is the big *n* problem, which imposes restrictions on the size of the matrices that have to be inverted in the model fitting process. This difficulty is overcome using a discrete approximation based on SPDEs. For some Gaussian random fields with Matérn covariance, SPDE provides an explicit link between the Gaussian random field and a discrete approximation based on a Gaussian Markov random field (GMRF) constructed on a triangulation, which can be used for computational purposes (Wist and Rue, 2006; Lindgren et al., 2011).

The SPDE approach allows a Gaussian field (GF) with the Matérn covariance function to be presented as a discretely indexed spatial random process (GMRF), which has significant computational advantages. Gaussian Fields are defined directly by their first- and second-order moments and their implementation is highly time-consuming, which leads to the so-called "big n problem". The idea is to construct a finite representation of a Matérn field by using a linear combination of basis functions defined in a triangulation of a given domain D. This representation leads to the SPDE approach, which is a link between the GF and the GMRF, and allows the spatio-temporal covariance function and the dense covariance matrix of a GF to be replaced with a neighborhood structure and a sparse precision matrix, respectively, both of which are typical elements that define a GMRF. This, in turn, yields substantial computational advantages (Lindgren et al., 2011).

More particularly, the SPDE approach consists in defining the continuously indexed Matérn GF X(s) as a discrete indexed GMRF by representing a basis function defined on a triangulation of domain D:

$$X(s) = \sum_{l=1}^{n} \varphi_l(s)\omega_l$$

where n is the total number of vertices in the triangulation; $\{\varphi_l(s)\}$ is the set of basis functions and $\{\omega_i\}$ are the zero-mean Gaussian distributed weights. The basis functions are not random, but are instead chosen to be piecewise linear on each triangle:

$$\varphi_l(s) = \begin{cases} 1 & at\ vertix \\ 0 & elsewhere \end{cases}$$

The key is to calculate $\{\omega_i\}$, which reports the value of the spatial field at each vertex of the triangle. The values inside the triangle will be determined by linear interpolation (Simpson et al., 2011).

The problem of the choice of the best mesh for the SPDE approximation could be solved using the correct steps presented in the next sections. The steps followed in this paper are: simulation, testing the different meshes, choice of the best one for each case, modeling, and comparing the results with DIC and WAIC.

3. Simulation

Working with all the possibilities in spatial point processes, first of all, the data are simulated and we have Regular, Cluster and Inhibition (Figure 1), which are simulated in a regular region (type A). For each case, the numbers of points are 462, 467 and 416, respectively.

Figure 1: Type A (first row) and Type B (second row). Regular, Cluster and Inhibition. Simulated by *lgcp* (third row).

For the second type that was simulated (type B), we have an irregular region and, in this case, the numbers of points are 329, 269 and 250, respectively. The structure of the irregular region is the province of Castellón in the Valencian Community, Spain. Finally, the third row are the data simulated by *rLGCP* function of *statstat* package. In the last possibility, the data is simulated directly as Log Gaussian Cox Process as another different possibility.

The statistical description of the variables data is presented in Figure B1 in the Appendix B, with the Figures B2 and B3. These are related to the spatial distances, the most important component for the study of spatial point processes. The histogram of the distances between sites and the cumulative proportion are also shown for each case. It shows we have all types of distances in the data, which is the normal structure for spatial point processes.

SPDEs for each pattern

The next step is to choose the best mesh for the distribution of each database using SPDE. When the mesh is prepared, it is possible to use two different codes, including (or not) *inla.nonconvex.hull*. Indeed, the use (or not) of the boundary increases the number of cases. Next Figure shown the elements studied in this process (Figure 2). It is possible to see in the first line the mesh on the left and the vertex numbered on the right. In the second line, each element of the mesh separated.
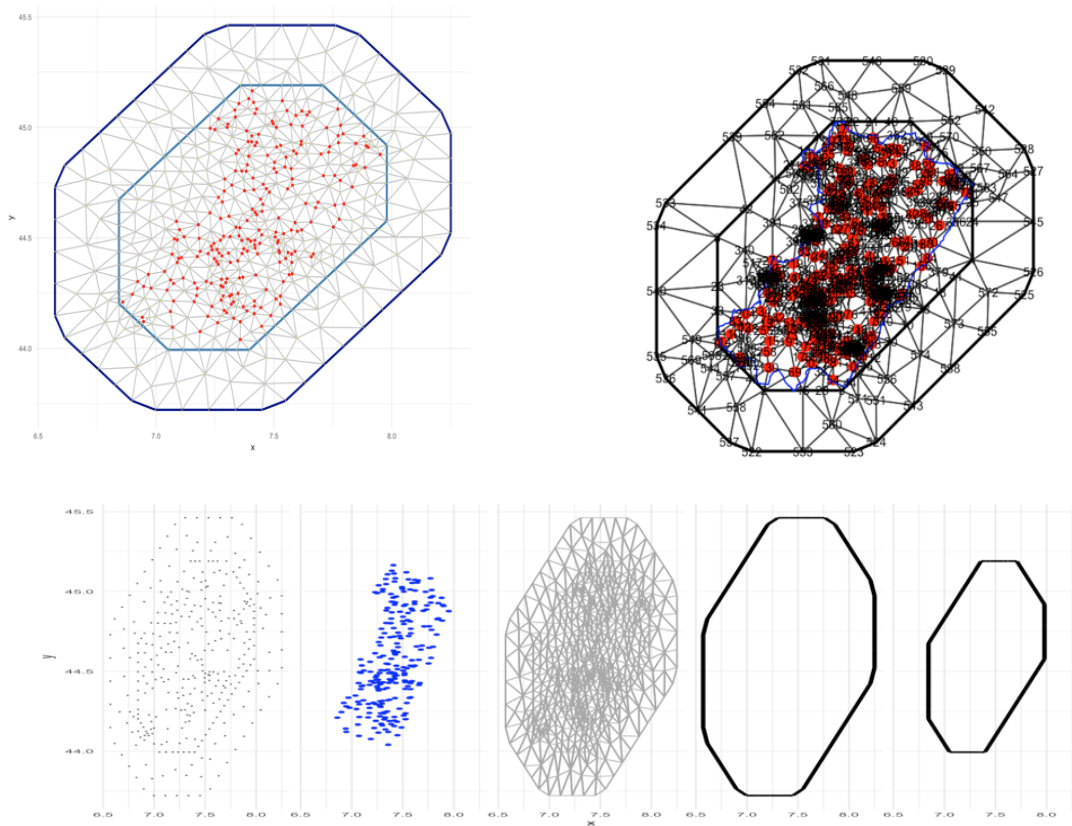
Figure 2: Mesh elements in SPDE. First line the mesh (left) and vertex numbered (right). Second line the elements of the mesh.

In the same way, next Figures shown the possibilities for control the mesh presented by SPDE-INLA (Figures 3 to 5) with the corresponding table for the parameters (Table 1 to 3).
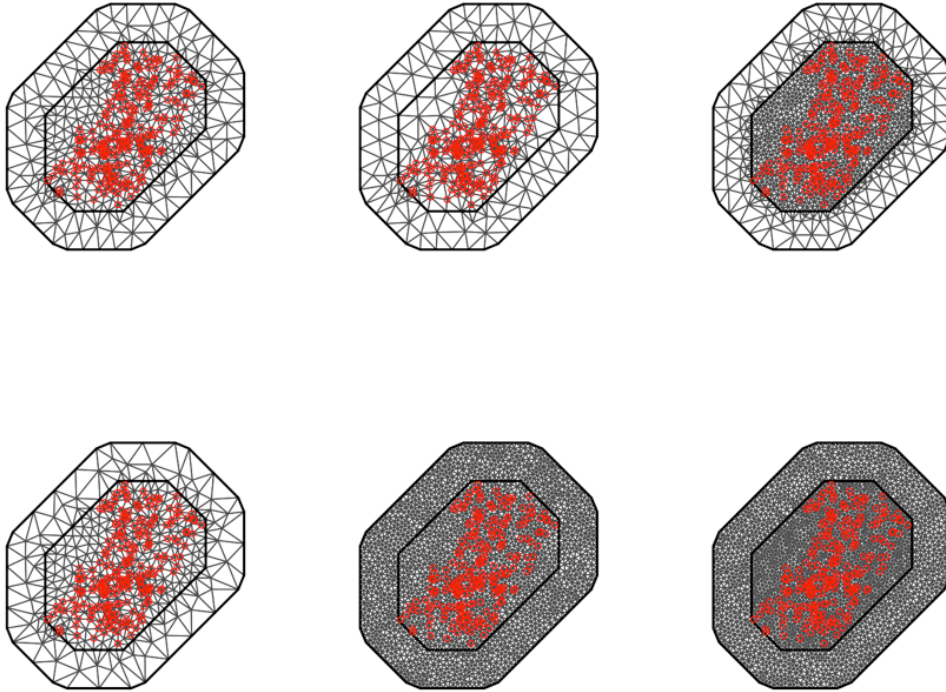
Figure 3: Meshes with *max.edge* changed.

	Mesh 1	Mesh 2	Mesh 3	Mesh 4	Mesh 5	Mesh 6
Max.edge	0.1; 0.2	0.2; 0.2	0.05; 0.2	0.1; 0.5	0.1; 0.05	0.04; 0.05
Cutoff	0.01	0.01	0.01	0.01	0.01	0.01
Offset	0; -0.2	0; -0.2	0; -0.2	0; -0.2	0; -0.2	0; -0.2
Number vertex	575	501	1259	551	2373	2908

Table 1: Parameters for Meshes 1 - 6.
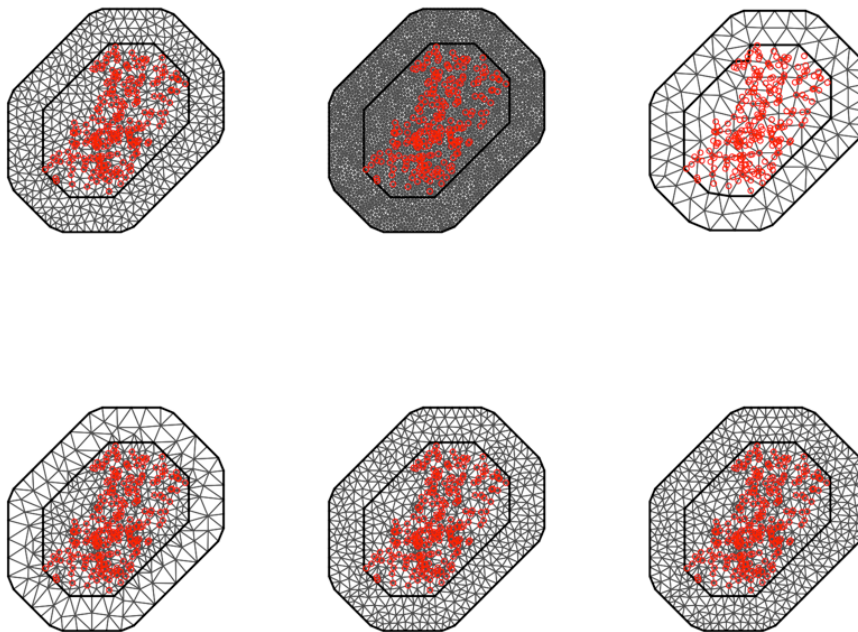
Figure 4: Meshes with *max.edge* changed, and *cutoff*.

	Mesh 7	Mesh 8	Mesh 9	Mesh 10	Mesh 11	Mesh 12
Max.edge	0.1	0.04	0.1; 0.2	0.1; 0.2	0.1	0.01
Cutoff	0.01	0.01	0.1	0.001	0.001	-0.001
Offset	0; -0.2	0; -0.2	0; -0.2	0; -0.2	0; -0.2	0; -0.2
Number vertex	795	3569	154	681	916	916

Table 2: Parameters for Meshes 7 - 12.
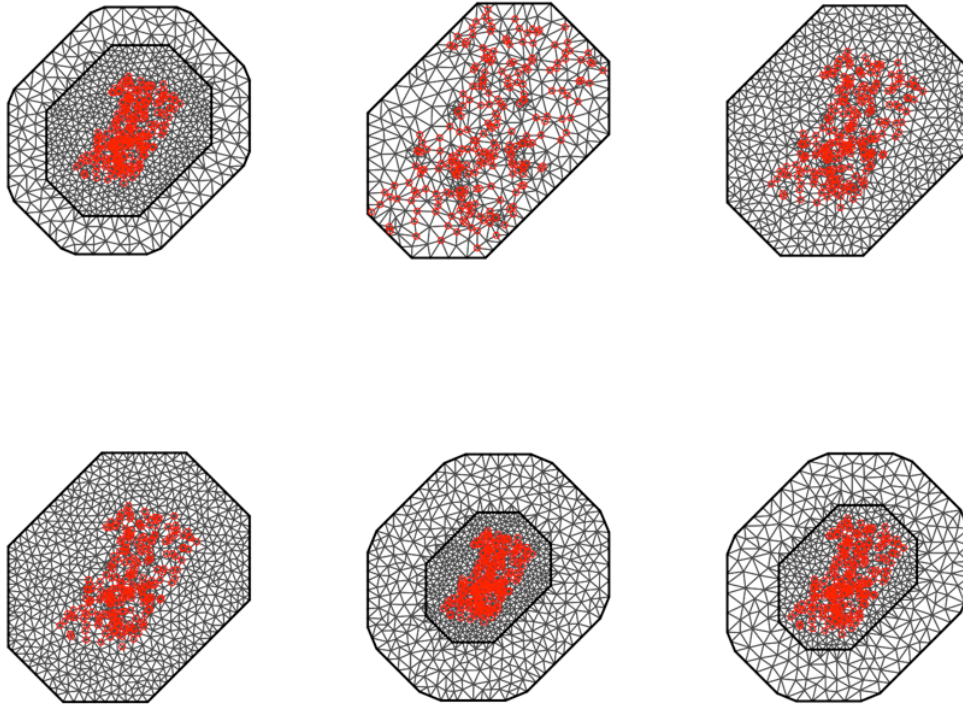
Figure 5: Meshes with *max.edge, cutoff and offset* changed.

	Mesh 13	Mesh 14	Mesh 15	Mesh 16	Mesh 17	Mesh 18
Max.edge	0.1; 0.2	0.01	0.1	0.1	0.1; 0.2	0.1; 0.2
Cutoff	0.01	-0.001	-0.001	-0.001	0.01	0.01
Offset	0.3; -0.2	0	0.3	-0.3	0.2; -0.4	0.1; 0.5
Number vertex	575	583	929	1077	1030	783

Table 3: Parameters for Meshes 13 - 18.

The different number of meshes is 11 possibilities for each regular and irregular region, with Regular, Cluster and Inhibition data, thus resulting in a total of 66 meshes. Figures B4 to B9 in Appendix 2 show the different meshes, with the meshes wiht *lgcp* function presented in Figures B10 to B11.

In the case of irregular regions, the mesh can be produced in three ways: using only data, only the boundary or both of them together. In our case, we have used the last one, for the best model. If all the possibilities are presented, the total number of meshes is double. The numbers of vertices for each case are presented in Table 4. The dispersion in the number of vertices in each mesh is what really makes it difficult to select the best mesh.

	Regular Data	Inhibition Data	Cluster Data
Regular region	927; 103; 681; 1133; 927; 44; 61; 927; 73; 73; 82; 46; 429 (Figure 4)	896; 896; 896; 1340; 1659; 850; 1312; 935; 77; 77; 88; 144; 1253 (Figure 5)	1100; 101; 732; 1343; 1141; 31; 65; 1100; 75; 75; 72; 49; 559 (Figure 6)
Irregular region	732; 90; 566; 748; 732; 36; 55; 1000; 72; 84; 69; 42; 454 (Figure 7)	595; 128; 499; 617; 671; 103; 60; 829; 84; 84; 69; 42; 208 (Figure 8)	708; 129; 479; 684; 787; 100; 53; 972; 84; 84; 69; 42; 208 (Figure 9)
Lgcp Regular	Regular region 795; 107; 657; 1032; 795; 38; 69; 1037; 80; 80; 74; 34; 450	Irregular region 537; 84 420; 574; 537; 39; 59; 840; 84; 76; 66; 40; 375	

Table 4: Number of vertices for each case.

For each case, it is necessary to decide on the best mesh. It depends on the number of points, computing time and if the data are inside the region. In the next step it will be selected with the DIC and WAIC. The next figure shows the 18 meshes selected, and the characteristics of each case can also be seen. The conditions and the differences between the best and the worst selected for each case can be observed. The differences and the importance of choosing the best mesh for modeling are quite apparent. The same is done with the data simulated with *lgcp* function of *spatstat* package. The 9 meshes selected for the regular regions are in Figure 6 (a-b).
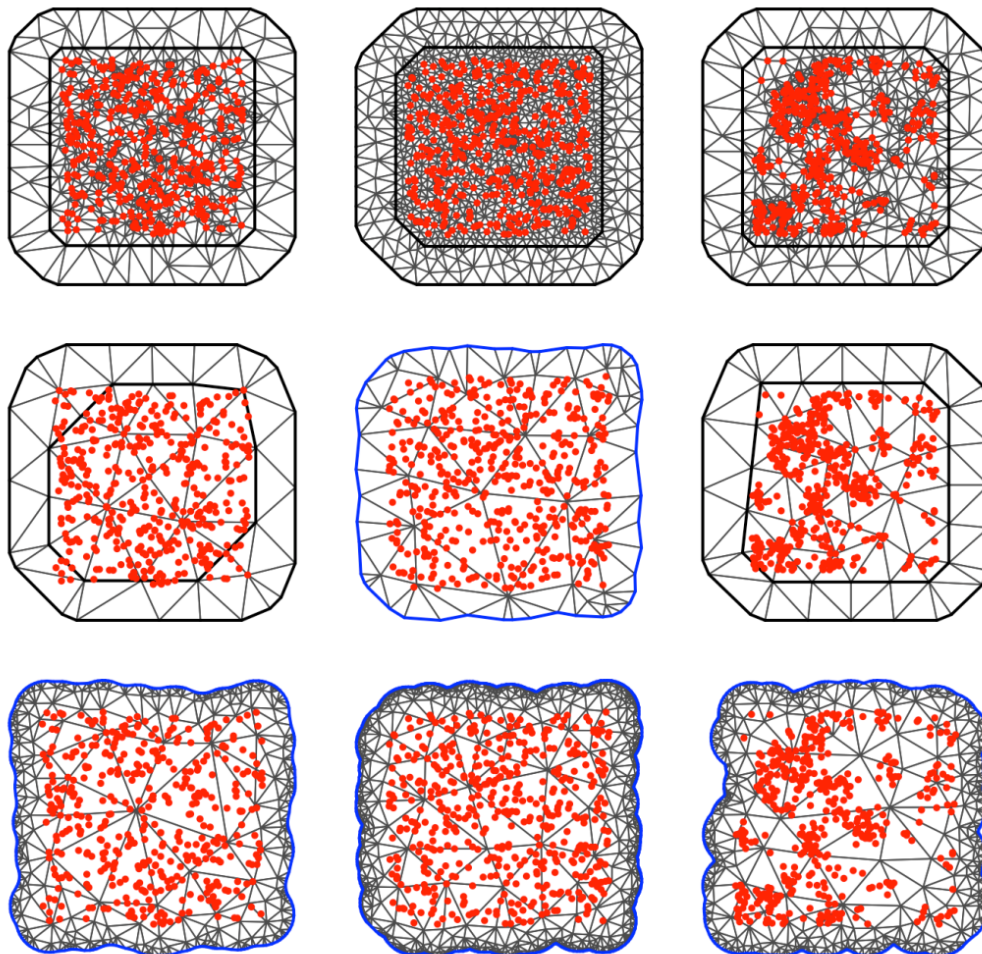
Figure 6a: The 9 meshes selected for a regular region.
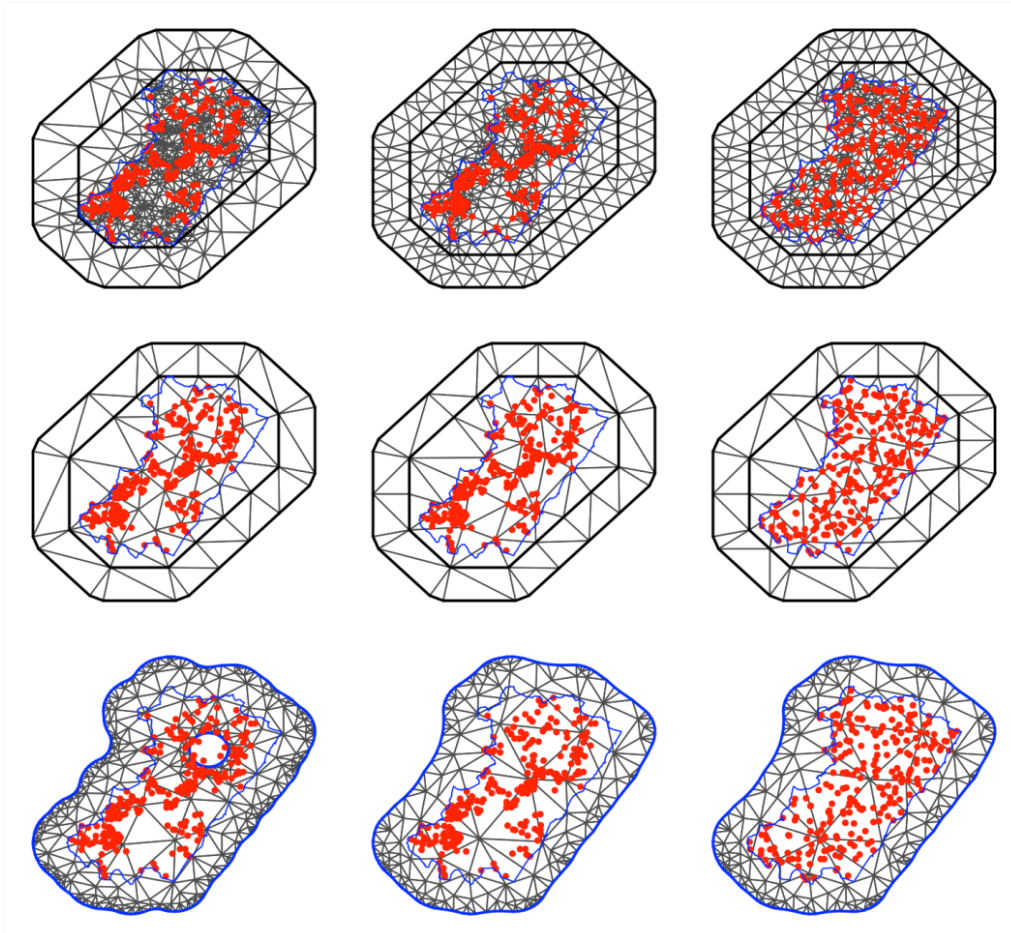
Figure 6b: The 9 meshes selected for an irregular region.

4. Applied models

The next step is to develop the models for each case and to decide on the best one. For all cases, the models are presented with and without a spatial effect (In Table 5 the time in seconds of computation of each model is presented). For this reason, the number total of possibilities is twice that of the previous step.

For the simulation steps, two covariates are presented, both Normal distributed. Indeed, one of them is the response variable and the other, with the product of the two of them, are the two sample covariates. The different components and information for the initial case are presented in the first part. Then, all the other cases are presented together.

Case A: Regular Data with Regular region using the meshes selected in previous steps (Models M1-M3).
Case B: Regular Data with Irregular region using the meshes selected in previous steps (Models M4-M6).

	Model 1	Model 2	Model 3	Model 4	Model 5	Model 6
Non-spatial effect	3.4882	1.7259	2.1738	1.6832	1.5079	1.4386
Spatial effect	7.5670	4.0028	6.9747	6.9506	3.8036	5.3732

Table 5: Time in seconds.

The effect that variations in each simulated covariate had on the response variable was analyzed. For this purpose, INLA were obtained using the freeware statistical package R (version 3.4.3) and the R-INLA package. Models were obtained separately with or without spatial effect.

The variable response was modeled against each covariate. Models are reported in Table 6, where the structure of each model is shown in:

$$Y = \beta_0 + \beta_1 V1 + \beta_2 V_1 V_2$$

Each cell in Table 6 reports the model for the simulated data, and for the response variables V_1 and V_1*V_2. In the same way, in this Table are presented the results for models M7: *lgcp* regular region and M8: *lgcp* irregular region data. The results are similar than the previous models (M1 to M6).

	β_0 Mean [0.025 quant, 0.975 quant]	β_1 Mean [0.025 quant, 0.975 quant]	β_2 Mean [0.025 quant, 0.975 quant]
M1 - Non-Spatial effect	19.9561 [19.8591; 20.0530]	0.4667 [0.1027; 0.8304]	-0.0231 [-0.0413; -0.0041]
M1 - Spatial Effect	19.9574 [19.8574 ;20.0574]	0.4657 [0.1003; 0.8308]	-0.0230 [-0.0413; -0.0047]
M2 - Non-Spatial effect	19.9561 [19.8591;20.0530]	0.4667 [0.1027; 0.8304]	-0.0231[-0.0413; -0.0049]
M2 - Spatial Effect	19.9563 [19.8542; 20.0583]	0.4676 [0.1039; 0.8309]	-0.0231 [-0.0413; -0.0049]
M3 - Non-Spatial effect	19.9561 [19.8591; 20.0530]	0.4667 [0.1027;0.8304]	-0.0231 [-0.0413; -0.0049]
M3 - Spatial Effect	19.9565 [19.8549; 20.0580]	0.4678 [0.1038; 0.8315]	-0.0231 [-0.0413; -0.0049]
Hyperparameters for M1 with spatial effect	κ = 35.95037	σ = 0.08259	r = 0.101414
Precision for the Gaussian observations M1	τ= 1.913073	σ = 1.003121	
M4 - Non-Spatial effect	19.994 [19.8875, 20.1006]	-0.0011 [-0.4354, 0.4328]	0.0004 [-0.0212, 0.0219]
M4 - Spatial Effect	19.9951 [19.8848, 20.1053]	0.0011 [-0.4337, 0.4355]	0.0002[-0.02135, 0.0218]
M5 - Non-Spatial effect	19.9941 [19.8875, 20.1006]	-0.0011 [-0.4355, 0.4328]	0.0004 [-0.0212, 0.0219]
M5 - Spatial Effect	0.0056 [-62.082, 62.0415]	-0.0010[-0.444, 0.4419]	0.0003 [-0.0216, 0.0223]
M6 - Non-Spatial effect	19.994 [19.8875, 20.1006]	-0.0011[-0.4354, 0.4328]	0.0003 [-0.02121, 0.0219]
M6 - Spatial Effect	19.9995 [19.8822, 20.1191]	0.00001 [-0.4352, 0.4349]	0.0002 [-0.0213, 0.0219]
Hyperparameters for M4 with spatial effect	κ = 317.6976	σ = 0.04487588	r = 0.07875396
Precision for the Gaussian observations M4	τ= 1.755458	σ = 0.982564	
M7 - lgcp -regular - Spatial effect	19.662[9.5139,27.0881]	0.0002[-0.0205, 0.0209]	
M7 - lgcp -regular - Non-Spatial effect	20.0291[19.9250,20.1330]	0.0004[-0.0205, 0.0212]	
M8 - lgcp -irregular - Spatial effect	19.5897[9.5736,26.4373]	-0.0395[-0.0674, -0.0116]	
M8 - lgcp -irregular - Non-Spatial effect	20.0219{19.8871,20.1566]	-0.0287[-0.0665, -0.0110]	
Hyperparameters for M7, M8 with spatial effect	κ = 0.59186 κ = 0.5939	σ = 0.34376 σ = 0.288307	r = 7.809422 r = 10.68171
Precision for the Gaussian observations M7, M8	τ= 1.897201 τ= 1.65136	σ = 1.028346 σ = 1.05865	

Table 6: Intercept and the fixed effects (β_i) for the models by considering each response variable against each covariate. The hyperparameters are included.

If the parameters are compared for non-spatial or spatial effect, it is clear that there are not many differences (Figures 7 and 8).
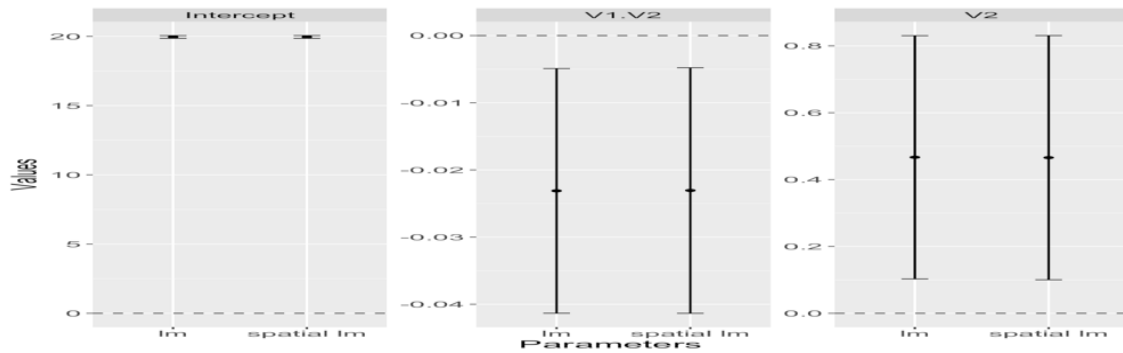

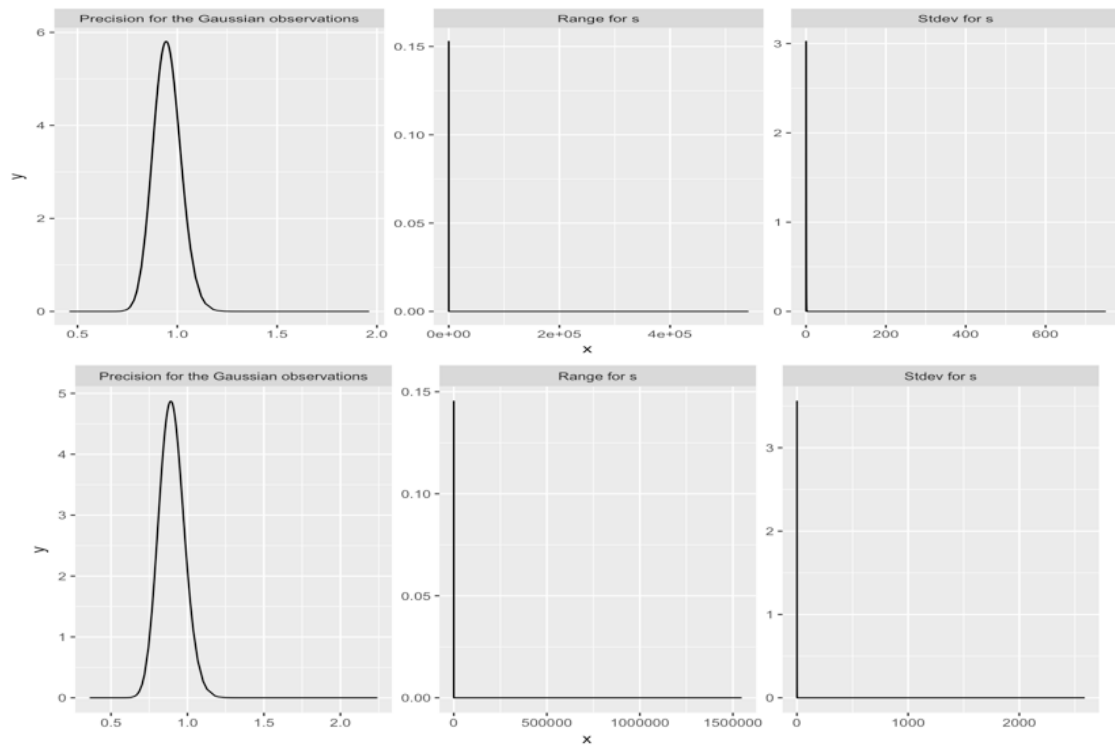Figure 7: Comparison of model parameters.

Figure 8: Parameter structure for regular (first row) and irregular (second row) in *lgcp* data.

On the other hand, DIC and WAIC are presented with the same information so as to allow comparison among the models. Table 7 shows the summary results related to goodness-of-fit for the battery of models.

	DIC	WAIC
M1 - Non-spatial effect	1188.787	1190.530
M1- Spatial effect	1188.317	1190.212
M2 - Non-spatial effect	1188.788	1190.531
M2- Spatial effect	1188.862	1190.632
M3 - Non-spatial effect	1188.788	1190.530

M3- Spatial effect	1188.944 1190.624
M4 - Non-spatial effect	926.5833 929.0286
M4- Spatial effect	926.7945 929.1223
M5 - Non-spatial effect	926.5854 929.0288
M5- Spatial effect	924.6721 927.8104
M6 - Non-spatial effect	926.5810 929.0302
M6- Spatial effect	926.3983 928.7516
M7 - Non-spatial effect	1118.003 1117.812
M7 - Spatial effect	1116.516 1116.435
M8 - Non-spatial effect	714.4145 714.4474
M8 - Spatial effect	713.3403 713.3548

Table 7: DIC and WAIC of parameters all models.

It could be deduced from the results obtained that in both cases including a higher number of covariates improves the model because DIC and WAIC become lower, which indicates that these models allow better prediction. This was the case, for example, when we analyzed the values of DIC and WAIC for the three models that relate V_1 with every single covariate $V_1 * V_2$, therefore showing it is a better model.

The next step is to study the spatial effect, in two formats: normal and 3D. This is presented in Figure 9a and 9b.
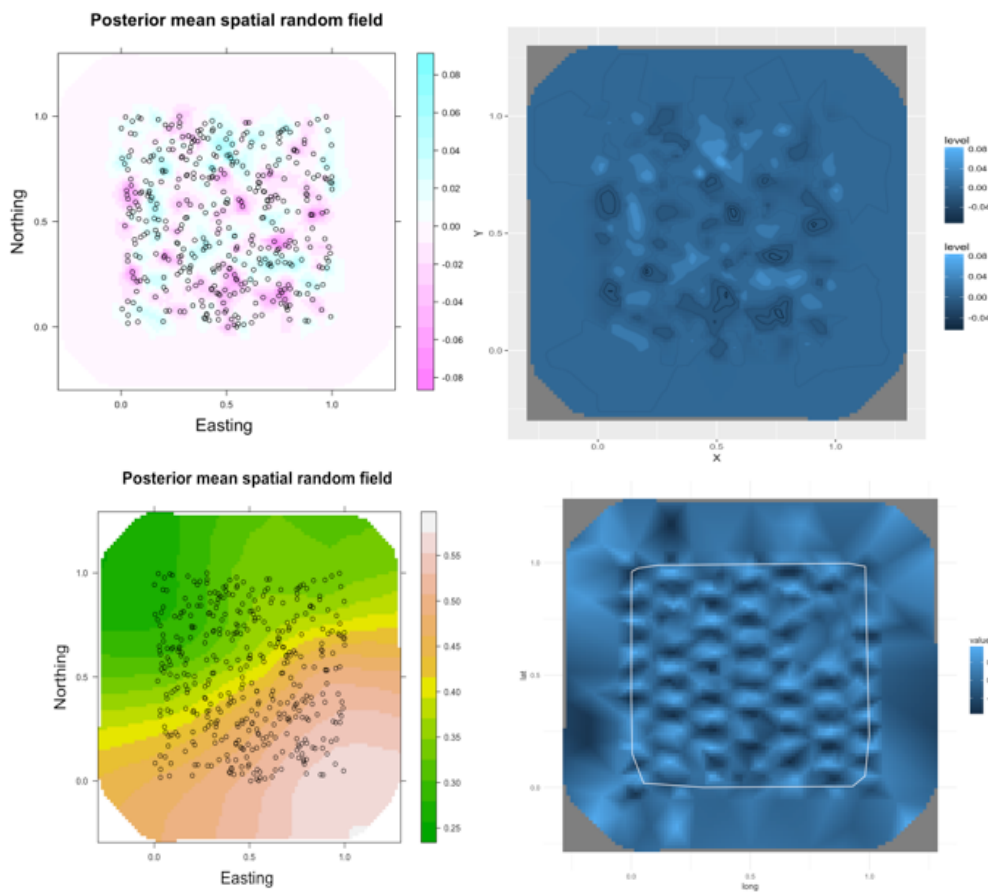
Figure 9a: Spatial effect: Regular region for *lgcp*.
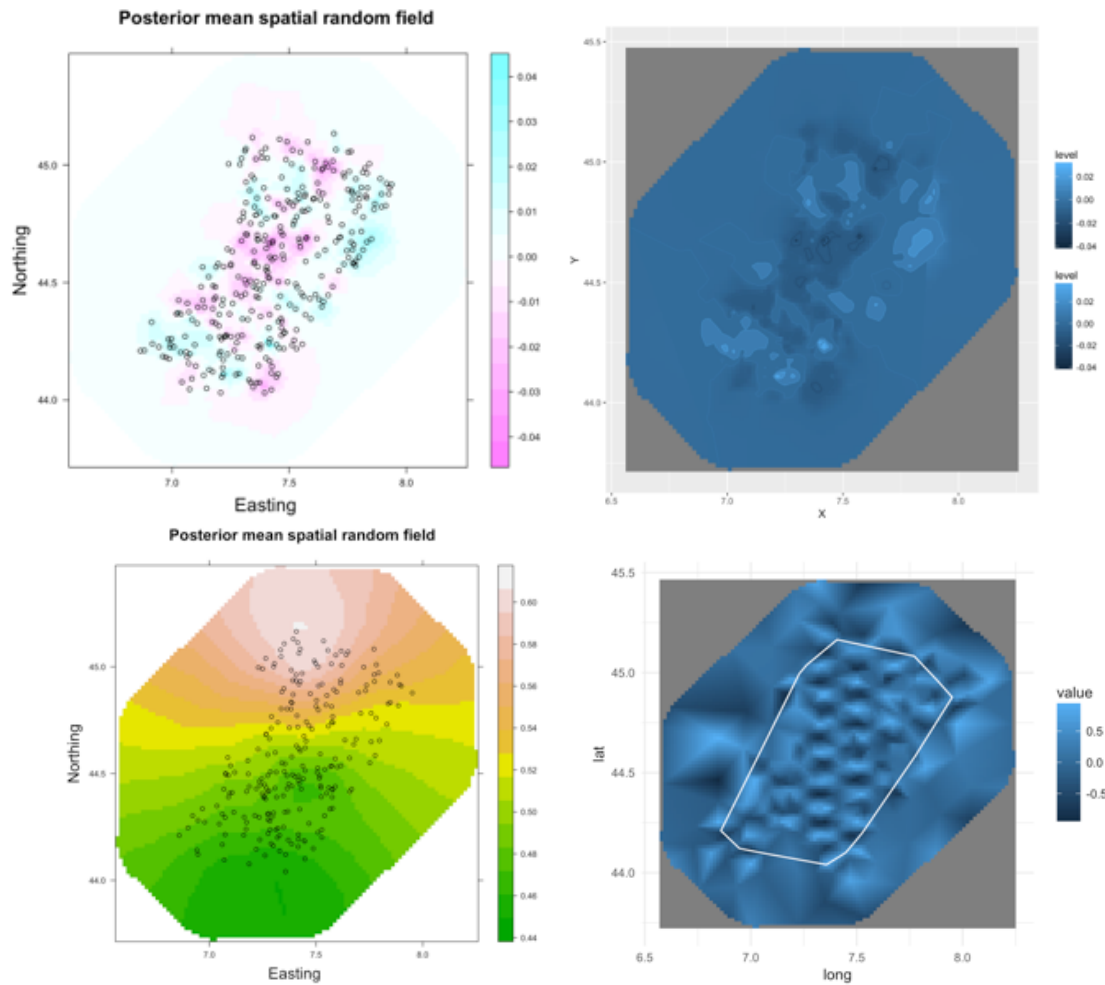
Figure 9b: Spatial effect: Irregular region *lgcp* simulated.

By means of the corresponding model parameters, the spatial effect can be presented, showing the correlation with the corresponding distance (Figure 10).
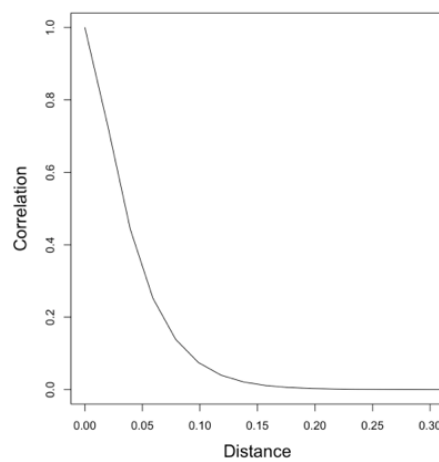
Figure 10: The correlation depending on the distance in the model.

A previous step for prediction is validation. This is performed by comparing the residuals and real data, and comparing prediction and real data, as can be seen in Figure 11 below.
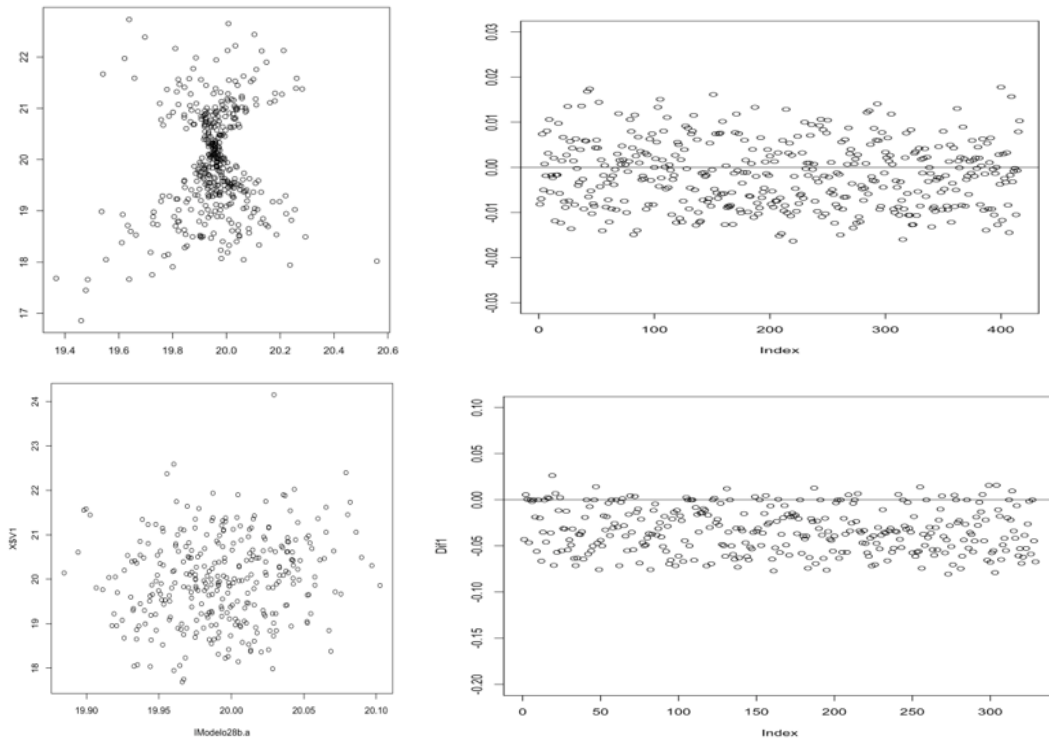
Figure 11: Residual comparison (left), real–predicted differences (right).

The residuals for *lgcp* data simulated are shown in next Figure 12:
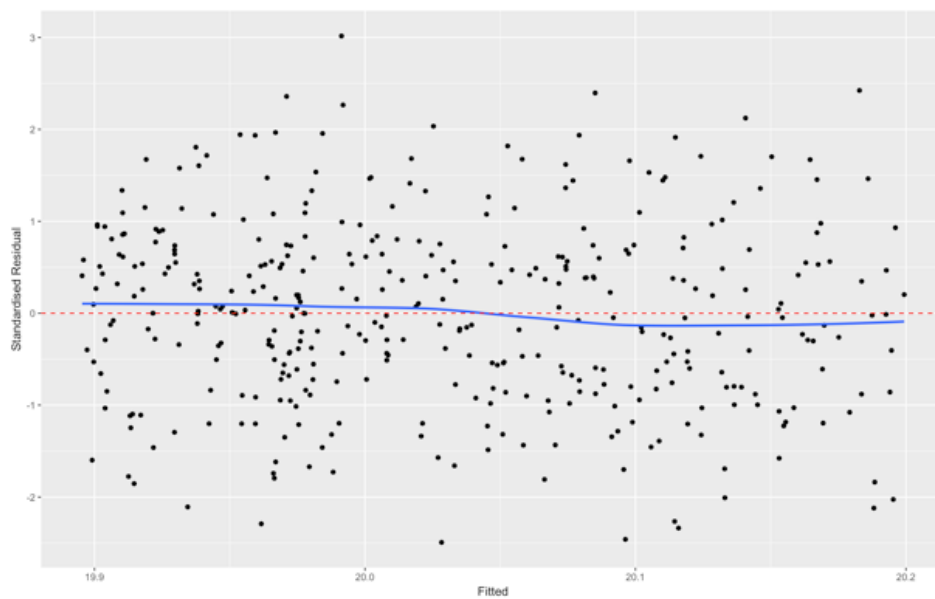
Figure 12: Standardized Residuals vs. fitted values.

In the next step, the simulated data could be presented, together with the predicted model and the related standard deviation. It is shown in the next Figure 13 for a regular and irregular case for *lgcp*. The other cases are shown in Figure B12 in the Appendix.
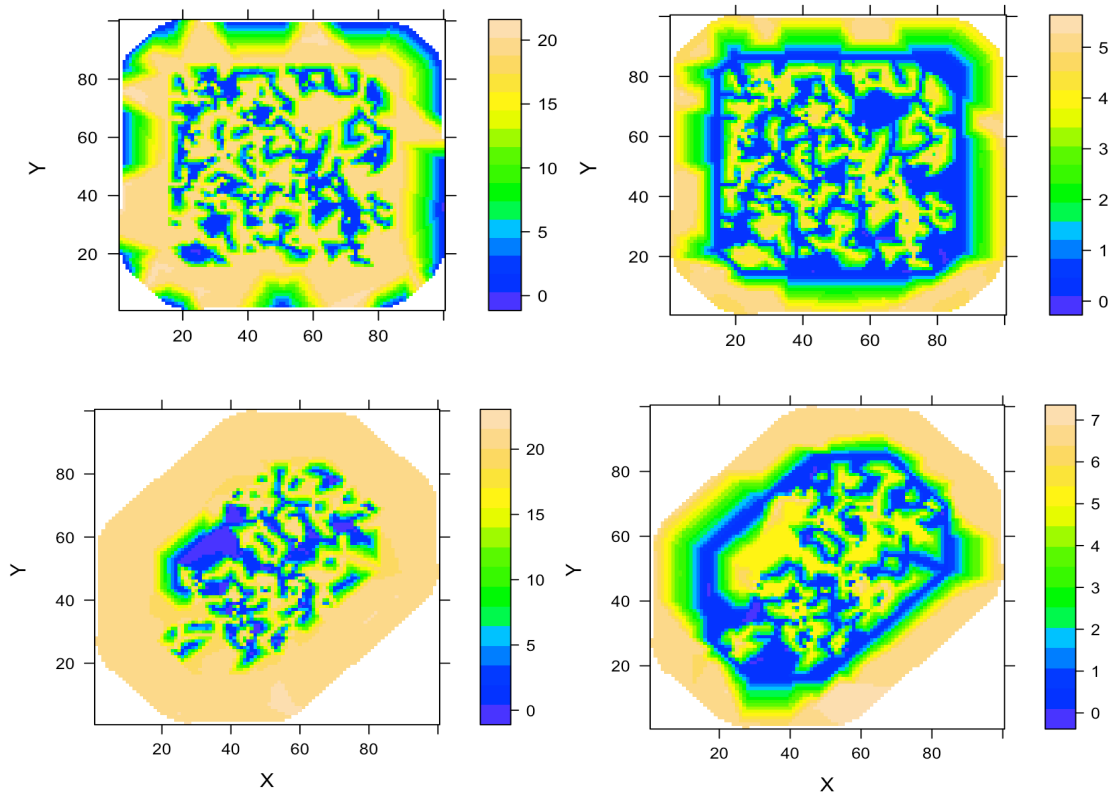
Figure 13: Value models for regular region with *lgcp* data (first row) and irregular region (second row).

The code for all steps is presented in Appendix A.

5. Real Data. Burned area in wildfires

A wildfire is any uncontrolled fire in combustible vegetation that occurs in the countryside or a wilderness area (Cambridge, 2008). A wildfire differs from other fires by its extensive size, the speed at which it can spread out from its original source, its potential to change direction unexpectedly, and its ability to jump gaps such as roads, rivers, and fire breaks (National Interagency Fire Center, 2011). Wildfires are characterized in terms of the cause of ignition, their physical properties such as speed of propagation, the combustible material present, and the effect of weather on the fire (Flannigan et al., 2006).

Fire risk is very important in the Mediterranean region because it has a marked seasonality, with high temperatures and low humidity in summer. Climatic trends interact with the landscape dynamics. The process of afforestation of the different agricultural areas with the increasing abandonment of rural activities has led to a situation of extreme vulnerability to the risk of fires, especially in mountainous Mediterranean areas, where this has led to abandonment and still represents an expansion, accumulation and greater continuity of the forest. In addition, other factors such as the development of second homes in these forest areas, the proliferation of roads and electricity networks, and an increased presence of human beings make this countryside more prone to suffer large forest fires due to the fact that they facilitate the process of starting fires (Díaz-Delgado and Pons, 2001; Moreira et al., 2001).

Given that wildfires are a natural element of the Mediterranean ecosystem, the prevention and suppression of forest fires should be addressed in order to lower the risk and vulnerability levels to values that are tolerable for society.

If every wildfire is associated with its spatial coordinates, longitude and latitude of the centroid of the burned area or the place where it was detected, along with other variables such as size or cause of the forest

fire, and controlling for the moment in time in which it was produced, one can identify all wildfires with a spatial-temporal stochastic process. Such processes, called spatial point processes, often display dependence between the spatial positions and moments in time, and interdependence between them. What is usually of more interest is the detection of trends in the intensity of fire locations, and determination of how (or whether) such trends are influenced by covariates, observable at each location of the spatial window. These covariates might include vegetation or land use, other descriptors of terrain (such as elevation, slope and orientation), and still others such as proximity to concentrations of human population or to concomitants of human activity (roads and railroads). Interaction between points may in general be of some interest in its own right. More important is the impact of the presence of interaction on statistical inference concerning trends and their dependence upon covariates. Temporal clustering of wildfires, whether deriving from multiple ignition lightning events, arson (Butry and Prestemon, 2005), or other sources, combined with favorable fuel and weather conditions, can force suppression resource rationing across space. Spatial clustering can also indicate the presence of risk factors.

Data setting

We analyze the patterns produced by wildfire incidents in the Valencian Community, located on the northeast coast of the Iberian Peninsula. The region is bordered by Catalonia to the north and the Iberian System range of mountains to the west. Furthermore, the region is delimited to the east by the Mediterranean Sea. It is a region with a surface area of 23,245 square kilometers, representing 4.6% of the Spanish national territory.

A total of 315 fires were recorded in the study area during 2015 (Figure 14). In addition to the locations of the fire centroids, in Cartesian coordinates (Mercator transversal projections, UTM, Datum ETRS89, zone 31-N), several covariates were also considered.
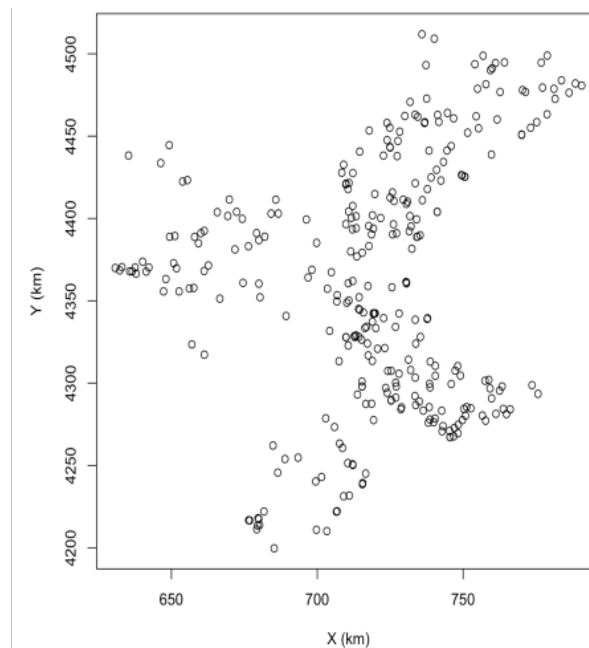

Figure 14: Distribution of forest fires in the Valencian Community in 2015.

The normal steps used for exploration of data in such cases are:

1) Data exploration
2) Outliers
3) Collinearity
4) Relationships Y vs. X
5) Variance Inflation factors

6) Interactions (is the quality of the data good enough to include them?)
7) Zero inflation justification.

The covariates, related to wildfires, used for the application are: typology, cause, causative, days last rain, temp_max (maxim temperature), Relative_H (Relative Humidity), wind speed, wind direction, combined model, danger degree, fire type, total tree, total not tree, Total (tree and not tree). The relationships between the covariates are shown in Figure 15 (boxplots).
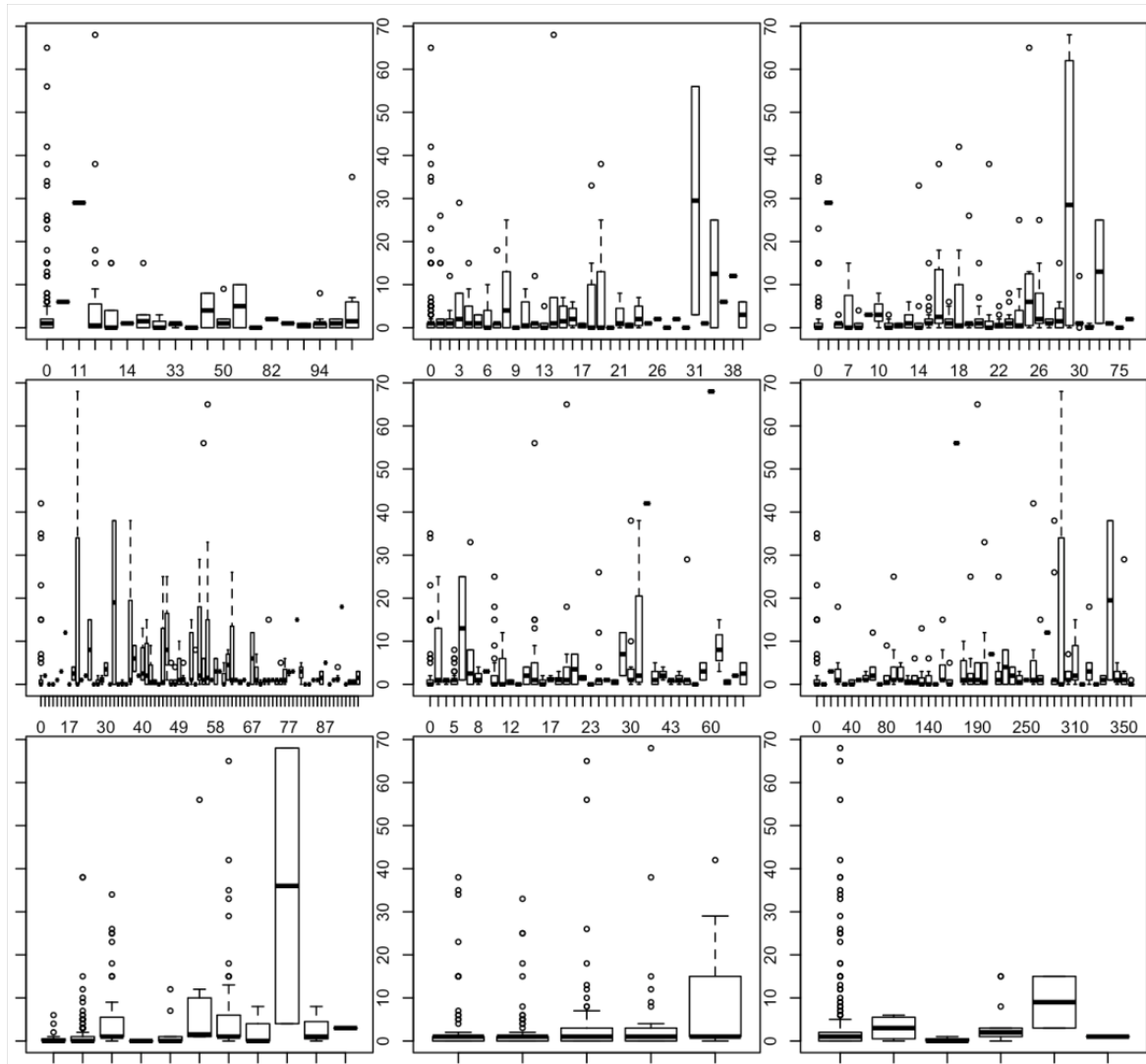

Figure 15: Boxplot covariates: cause, days last rain, temp_max, Relative_H, wind speed, wind direction, combined model, danger degree, fire type.

The next step is the Variance Inflation factors (GVIF), seeking the optimal variables and using only values below 2 because these are informative (Table 8).

	GVIF - Step 1	GVIF - Step 2
typology	1.060767	1.060414
group typology	2.441872	
cause	1.211273	1.080824
causative	2.444984	
days last rain	1.256075	1.221050
temp_max	1.520976	1.490312
Relative_H	1.412322	1.385338
wind speed	1.435472	1.435213
wind direction	1.690188	1.676258
combined model	1.182671	1.171493
danger degree	1.412806	1.393972
fire type	1.103011	1.100342
total tree	1.114397	1.107647
total no tree	1.199396	1.194232

Table 8: Values of GVIF in the two steps.

On representing the covariates in order to study the collinearity, no problematic structures or outliers are found. The next step, which is necessary for the study of real data, is the relationships. The most likely option to obtain patterns, however, is the relationship between each covariate and the response variable. In this case, the response variable is TOTAL (tree and not tree together). This is represented in Figure 16 and there is no pattern present.
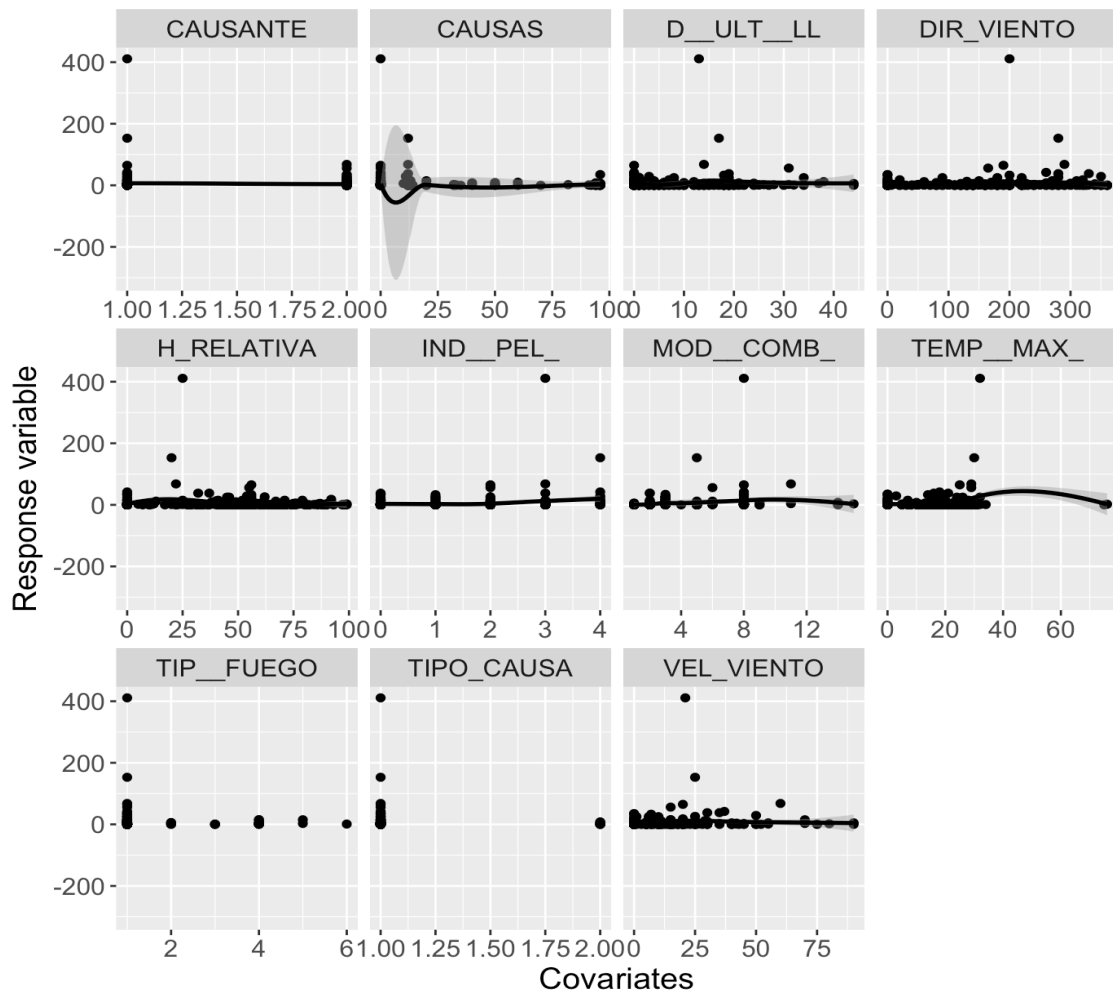
Figure 16: Response *vs.* covariates.

In the same way, the distances are studied, and different distances are found, which gives us the chance to continue the study including all of the referenced points (Figure 17).
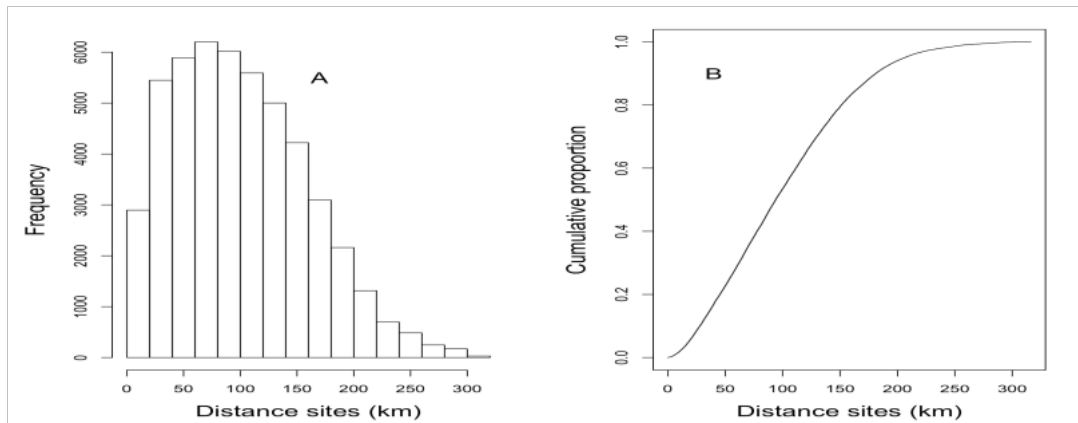

Figure 17: Frequency and cumulative proportion of distances.

Finally, before selecting the model, the decision regarding the model selected is important if the number of 0 in the data is high, since in this case the model will be Zero Inflation. There is 42.22% of zero data, and we will use a Zero-inflated model (Figure 18).
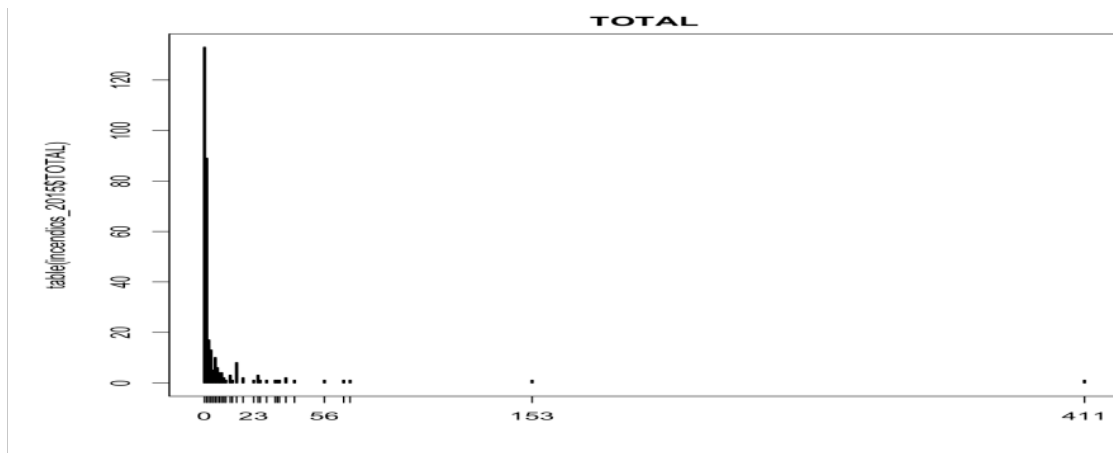
Figure 18: Values of response data.

Following the steps presented above, we use with simulations data is the SPDE, the same number of meshes, 9+4 (Figure 19) and Figure 20 below shows the two selected meshes.
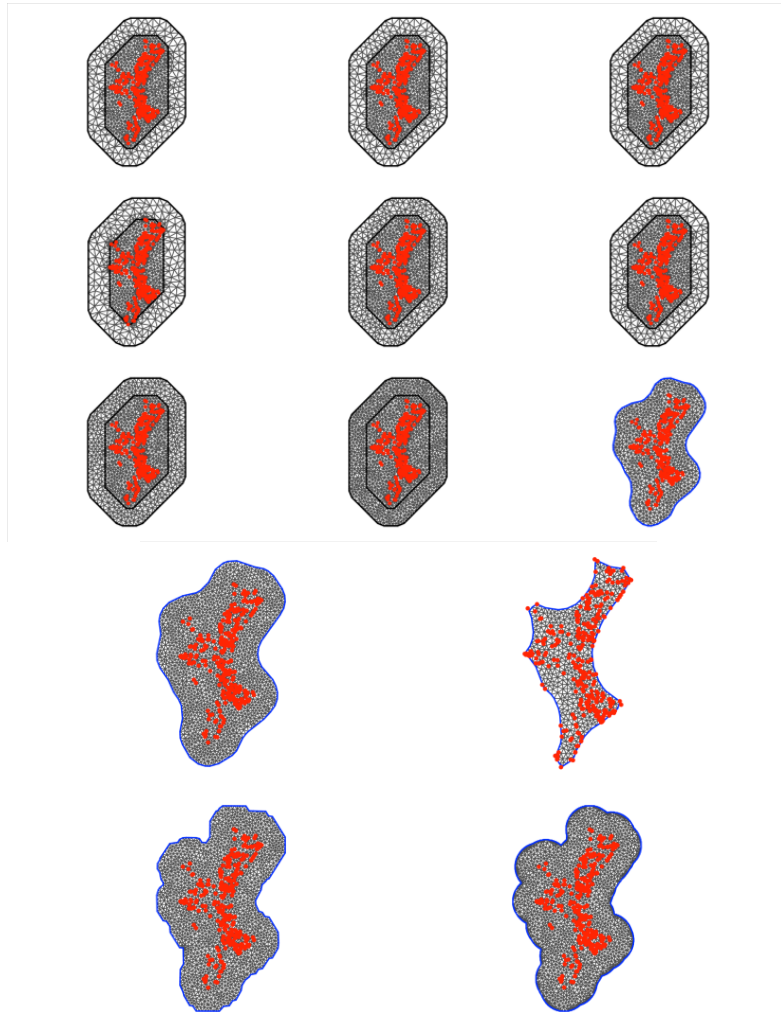
Figure 19: The 13 meshes, with respective numbers of vertices: 1612, 1430, 1612, 2021, 1732, 1356, 1592, 2071, 794, 1778, 600, 1836, 2801.
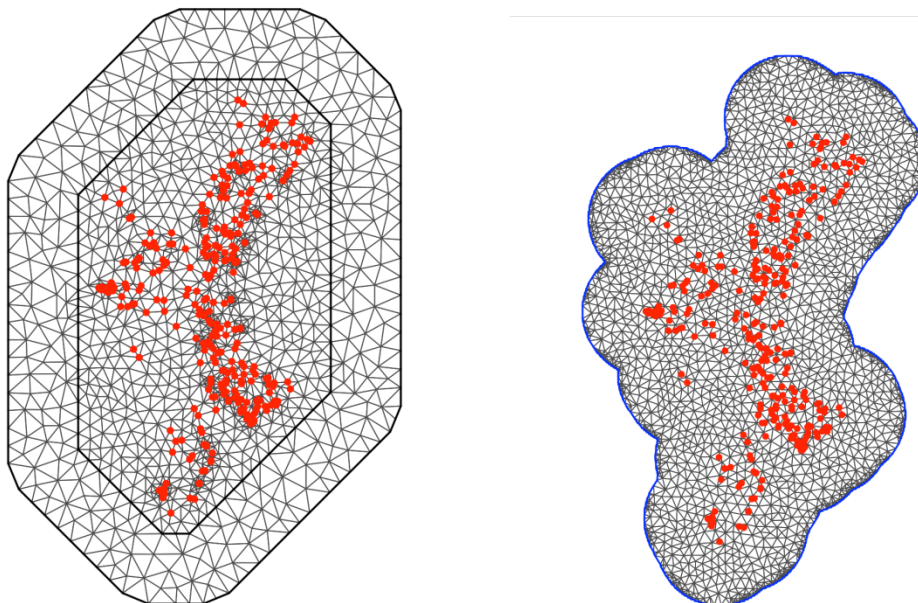

Figure 20: The meshes selected, with the previous steps.

The models applied for the real data, that is, wildfires in the Valencian Community in 2015, have both non-spatial and spatial effects and this affects the computing time (Table 9). Table 10 shows the value of the parameters for each model for real data. In Figure 21, the difference between the values of the parameters is apparent, and it is important for the final results.

	Model 1	Model 2
Non-spatial effect	1.7078	1.3112
Spatial effect	14.7019	23.9632

Table 9: Time in seconds.

|	β_0 Mean [0.025 quant, 0.975 quant]	β_1 Mean [0.025 quant, 0.975 quant]	β_2 Mean [0.025 quant, 0.975 quant]
M1 - Non-Spatial effect	2.2439 [2.1916, 2.2955]	-0.0352 [-0.0394, -0.0311]	0.0016 [0.00152, 0.0017]
M1 - Spatial Effect	0.2974 [-0.2243, 0.7566]	-0.0148 [-0.0300, -0.0002]	0.0025 [0.0015, 0.0036]
M2 - Non-Spatial effect	2.2439 [2.1917, 2.2955]	-0.0352 [-0.0394, -0.0311]	0.0016 [0.0015, 0.0017]
M2 - Spatial Effect	0.2384 [-0.3764, 0.7848]	-0.0163 [-0.029, -0.0039]	0.0033 [0.0022, 0.0045]
	$\kappa = 0.5166625$	$\sigma_u = 2.467049$	$r = 5.694205$

Table 10: Parameters of the model.
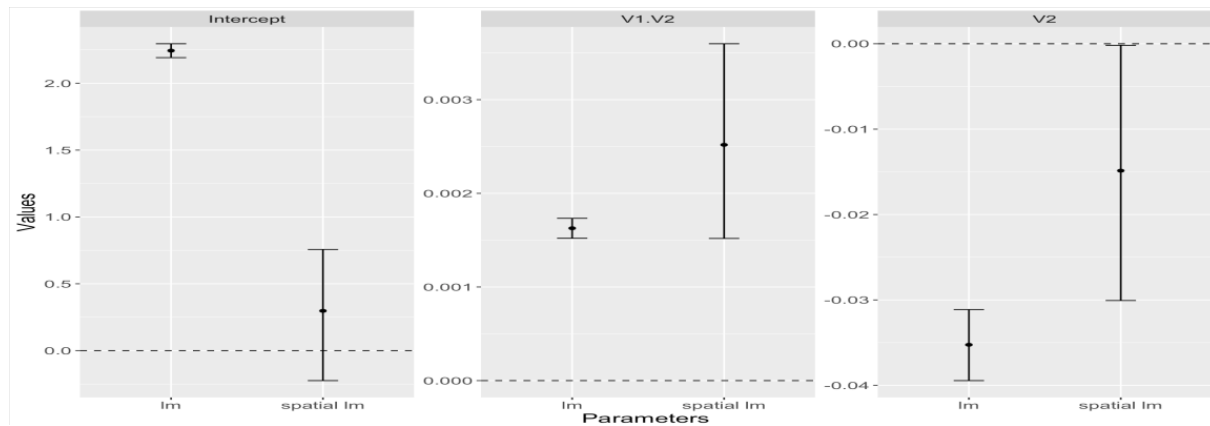
Figure 21: Comparison of parameters with and without spatial effect.

Table 11 below shows the summary results related to goodness-of-fit for the battery of models. DIC and WAIC.

	DIC	WAIC
M1 - Non-spatial effect	5183.299	4574.274
M1- Spatial effect	5184.681	4573.108
M2 - Non-spatial effect	1104.704	1131.896
M2- Spatial effect	-Inf	-Inf

Table 11: DIC and WAIC.

With these results, it can be deduced that including a higher number of covariates improves the model because DIC and WAIC become lower, which indicates that these models enable better prediction. Figure 22 shows the spatial effect of the Valencian Community in two formats.
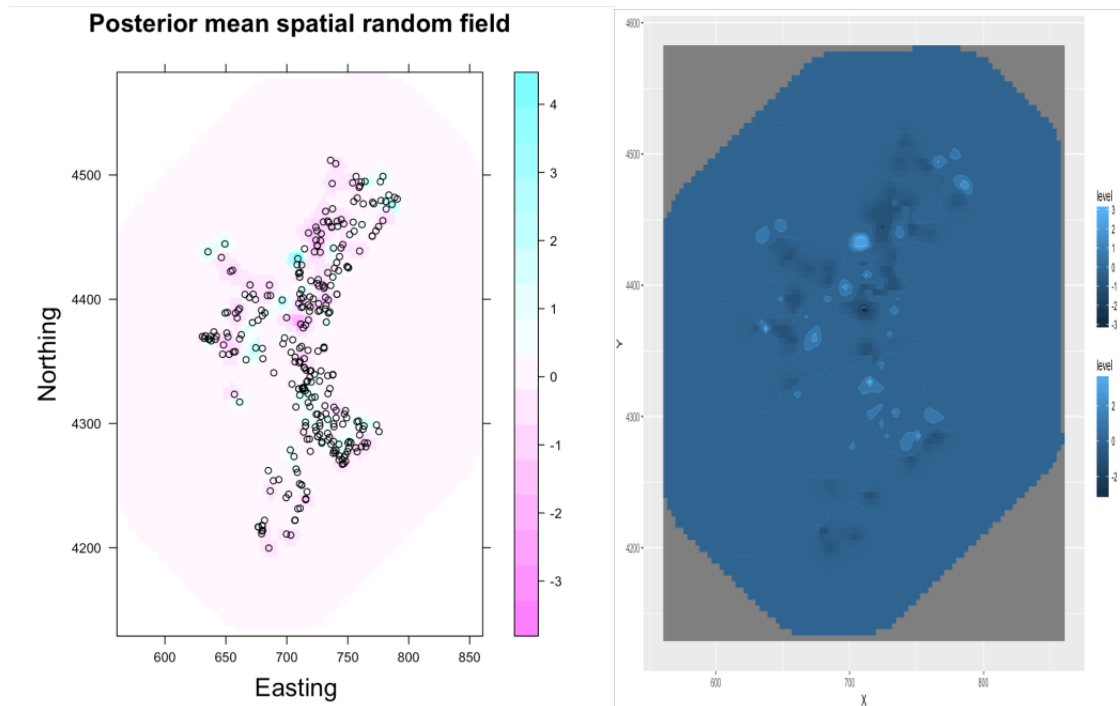

Figure 22: Spatial effect.

In this case, validation is performed by comparing residuals and with the correlation between the real data and the model data (Figure 23 up). The relationship with the distances can also be seen in Figure 23. The correlation in this case, $\rho = 0.8309389$, has a high value, which suggests a good result.
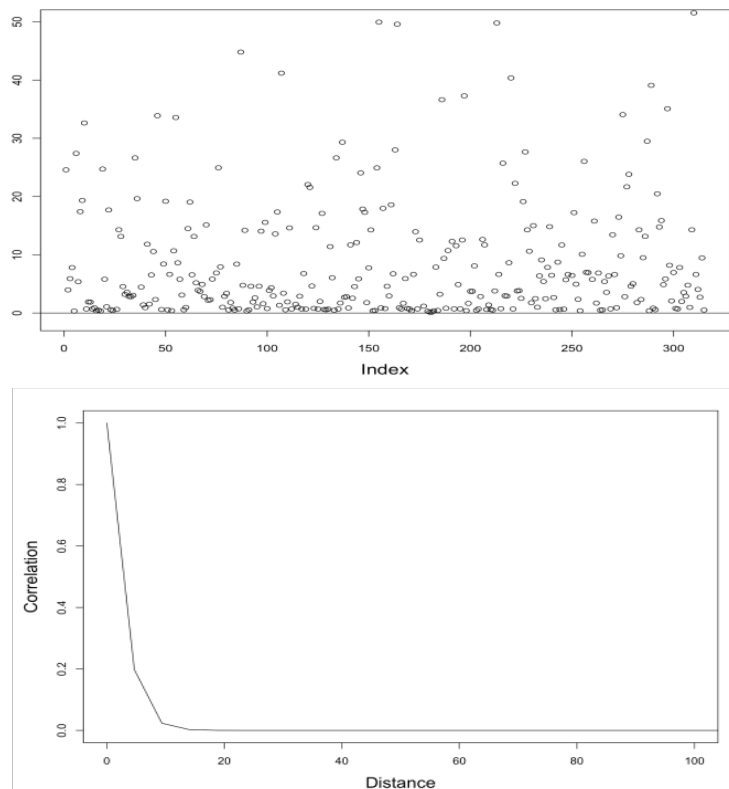

Figure 23: Differences between real and model data (up), and Correlation–distance (down).

6. Conclusions and Discussion

The problem of Bayesian Inference using SPDE for spatial point processes is considered in this work. The steps proposed for considering the best solution for each case are presented and modeled using simulated process models, where the latent Gaussian field is extended to a GRMF.

A computationally efficient method for Bayesian inference, based on INLA and SPDE, was presented. We looked at an application for modeling a wildfire dataset in which the process is faster and clearer. The example was of interest since the point pattern shows clear signs of being affected by some covariates and spatial elements.

In a more general context of spatial point process modeling, the data structure we considered here differs from the point patterns typically analyzed in the point process literature, but it is important to show that this SPDE methodology affords researchers easier and computationally efficient results. It is very important to note the steps used in the process and the reduction in computational time.

The advantage of INLA-SPDE is that it is able to predict the subsequent marginal distributions of the model parameters as well as the model responses without carrying out extensive simulations. This methodology can be potentially applied to mapping the spatial distribution of environmental variables or in all kinds of spatial point patterns. Therefore, the use of triangulated meshes in INLA-SPDE may lead to the possibilities of working with simple or complex databases.

The purpose of this study was to demonstrate that the use of the INLA-SPDE package (Rue et al., 2009, and Lindgren et al., 2011) to analyze all kinds of point patterns is faster, clearer, and computationally effective. The results showed that INLA-SPDE can also be a complementary tool in the wildlife biologist's analytical toolkit, where models are specified using a syntax that should be familiar to users of R, and where data are formatted in a straightforward way with relatively few lines of code.

As a conclusion, the SPDE methodology is a relevant element for the study of the spatial data, but it could be improved with the inclusion of the temporal effect as an element not separately with the space. In the same way, the spatial effect included in the model by SPDE is difficult because there are many elements included in this methodology and it is not well known by the researchers. It is shown in the results with wildfires because the small change in a parameter could modified the results. Nevertheless, the use of INLA-SPDE may lead to two possibilities, working with simple or complex databases, and this process can be potentially applied to mapping the spatial distribution of spatial data in all kinds of point patterns, in geostatistical data and including covariates.

7. References

Aragó, P., Juan, P., Díaz-Avalos, C., Salvador, P., (2016). Spatial point process modeling applied to the assessment of risk factors associated with forest wildfires incidence in Castellón, Spain. *Eur. J. For. Res*. http://dx.doi.org/10.1007/s10342- 016-0945-z.

Baddeley, A. and van Lieshout, M.N.M. (1995). Area-interaction point processes. *Ann Inst Stat Math* 47:601–619.

Barros, A.M.G., Pereira, J.M.C., 2014. Wildfire selectivity for land cover type: Does size matter? *PlosOne* 9 (1), e84760. http://dx.doi.org/10.1371/journal. pone.0084760.

Blangiardo, M., Cameletti, M., Baio, G. and Rue, H. (2013). Spatial and Spatio-temporal models with R-INLA. *Spatial and Spatio- temporal Epidemiology* 4:33–49.

Blangiardo, M., & Cameletti, M. (2015). *Spatial and Spatio-temporal Bayesian Models with R-INLA*. John Wiley & Sons.

Bivand R, Pebesma EJ, Rubio VG (2007) Applied spatial data analysis with R. Springer, New York

Butry DT, Prestemon JP. Spatio-temporal wildland arson crime functions. *American Agricultural Economics Association Annual Meeting*, 26–29 July 2005, Providence, Rhode Island, USA (available in: http://ageconsearch.umn.edu/handle/19197, accessed on March 7, 2011).

Cambridge Advanced Learner's Dictionary, Third Edition. Cambridge: Cambridge University Press, 2008.

Cameletti, M., Lindgren, F., Simpson, D., Rue, H., 2013. Spatio-temporal modeling of particulate matter concentration through the SPDE approach. *Adv. Stat. Anal*. 97 (2), 109–131.

Cressie, N.A., 1993. Statistics for Spatial Data. Wiley, New York.

Daley, D.J. and Vere-Jones, D. (2003). An Introduction to the Theory of Point Processes: Volume II: General Theory and Structure, volume 2. Springer. ISBN 0-387- 95541-0.

Diggle PJ (2003) Statistical analysis of spatial point patterns, 2nd edn. Arnold, London

Díaz-Delgado R, Pons X. Spatial patterns of forest fires in Catalonia (NE of Spain) along the period 1975–1995: *Analysis of vegetation recovery after fire. Forest Ecology and Management* 2001; 147(1):67-74.

Díaz-Avalos C, Peterson DL, Alvarado E, Ferguson SA, Besag JE (2001) Space-time modelling of lightning-caused ignitions in the Blue Mountains, Oregon. *Canadian Journal of Forest Research* 31:1579–1593

Díaz-Avalos, Carlos, Juan, Pablo and Serra-Saurina, Laura (2016). Modeling fire size of wildfires in Castellon (Spain), using spatiotemporal marked point processes. *Forest Ecology and Management* 381 (2016) 360–369

Ehlers, R and Zevallos, M. (2015). Bayesian Estimation and Prediction of Stochastic Volatility Models via INLA, *Communications in Statistics - Simulation and Computation*, 44:3, 683-693.

Flannigan MD, Amiro BD, Logan KA, Stocks BJ, Wotton BM. Forest fires and climate change in the 21st century. *Mitigation and Adaptation Strategies for Global Change* 2006; 11(4):847-859.

Juan, P., Saez, M., Mateu, J., 2012. Pinpointing spatio-temporal interactions in wildfire patterns. *Stochast. Environ. Res. Risk Assess*. 26 (8), 1131–1150.

Lindgren, F., Rue, H. and Lindstrom, J. (2011). An explicit link between Gaussian fields and Gaussian Markov random fields the SPDE approach. J. *Roy. Stat. Soc., Ser. B*, pp. 423-498

Mandallaz, D., Ye, R., 1997. Prediction of forest fires with Poisson models. *Can. J. For. Res*. 27, 1685–1694.

Martins, T., G., Simpson, D., Lindgren, F. And Rue, H. (2013). Bayesina computing with INLA: New features. Computational Statistics & Data Analysis, 67; 68-83.

Möller and Waagepetersen (2006). Statistical Inference and Simulation for Spatial Point Processes, Chapman and Hall/CRC, Boca Raton and London.

Møller, J., Díaz-Avalos, C., (2010). Structured spatio-temporal shot-noise Cox point process models, with a view to modelling forest fires. *Scand. J. Stat*. 37, 2–15.

Moreira F, Rego F, Ferrera P. (2001). Temporal (1958-1995) pattern of change in a cultural landscape of Northwestern Portugal: implications for fire occurrence. *Landscape Ecology*, 101:111-115.

National Interagency Fire Center. The Science of Wildland Fire (available in: http://www.nifc.gov/, accessed on February 14, 2011).

Neyens, T., Faes, C. and Molenberghs, G. (2018). Integrated nested Laplace approximation for the analysis of count data via the combined model: A simulation study, *Communications in Statistics - Simulation and Computation*. DOI: 10.1080/03610918.2017.1400053

R Core Team, 2016. R: A Language and Environment for Statistical Computing. R Foundation for Statistical Computing, Vienna, Austria.

R-INLA R-INLA project. <http://www.r-inla.org/home> (accessed on November 5th, 2017).

Rue, H., Martino, S. and Chopin, N. (2009). Approximate Bayesian inference for latent Gaussian models using integrated nested Laplace approximations (with discussion). *J. Roy. Stat. Soc. B,* 71, 319-392.

Ruiz-Cárdenas, R., Krainski, E.T. and Rue, H. (2012). Direct fitting of dynamic models using integrated nested Laplace approximations-INLA. Computational Statistics & Data Analysis. 56 (6), 1808-1828.

Spiegelhalter, D. J., N. G. Best, B. P. Carlin, and A. Van der Linde (2002). Bayesian measures of model complexity and fit (with discussion). *Journal of the Royal Statistical Society, Series B* 64 (4), 583–616.

Serra, L., Saez, M., Mateu, J., Varga, D., Juan, P., Diaz-valos, C., Rue, H., (2014a). Spatio- temporal log Gaussian Cox processes for modelling wildfire occurrence. The case of Catalonia, 1994–2008. *Environ. Ecol. Stat.* 21 (3), 531–563.

Serra, L., Saez, M., Juan, P., Varga, D., Mateu, J., (2014b). A spatio-temporal Poisson hurdle point process to model forest fires. *Stoch. Environ. Res. Risk Assess*. 28 (7), 1671–1684.

Simpson, D., Illian, J.B., Lindgren, F., Sørbye, S. H. and Rue, H. (2016). Going off grid: computationally efficient inference for log-Gaussian Cox processes, *Biometrika*, Volume 103, Issue 1, 49–70.

Tsanas, A., Xifara, A., (2012). Accurate quantitative estimation of energy performance of residential buildings using statistical machine learning tools. *Energy and Buildings*, 49, 560-567.

Taylor BM, Diggle P (2014). INLA or MCMC?. A tutorial and comparative evaluation for spatial prediction in log-Gaussian Cox processes. *Journal of Statistical Computation and Simulation*. 84(10):2266–2284

Vlad, Iulian, Juan, Pablo and Mateu, Jorge. (2015). Bayesian spatio-temporal prediction of cancer dynamics. *Computers and Mathematics with Applications*, 70, 857-868.

Xu, H., Schoenberg, F.P., (2011). Point process modeling of wildfire hazard in Los Angeles County, California. *Ann. Appl. Stat.* 5 (2A), 684–704.

Watanabe, S. (2010). Asymptotic equivalence of Bayes cross validation and widely applicable information criterion in singular learning theory. *Journal of Machine Learning Research* 11, 3571–3594.

Wist, h.T and Rue, H. (2006). Specifying a Gaussian Markov Random Field by a Sparse Cholesky Triangle, *Communications in Statistics - Simulation and Computation*, 35:1, 161-176.

Appendix A: CODE

The code presented is only for regular cases. The results of all cases, regular and irregular regions (two possibilities), are presented in the paper for Regular, Inhibition and Cluster data.

A) Data

```
# Regular:
myRegular <- rpoispp(400, win=owin(c(0,1),c(0,1)))
v1R=rnorm(length(myRegular$x), mean = 20, sd = 1)
v2R=rnorm(length(myRegular$x), mean = 0, sd = 5)
Regular=data.frame(x=myRegular$x,y=myRegular$y,v1R,v2R)

# Inhibition:
myStrauss <- rStrauss(0.05,0.2,1,square(100))
v1I=rnorm(length(myStrauss$x), mean = 20, sd = 1)
v2I=rnorm(length(myStrauss$x), mean = 0, sd = 5)
Inhibition=data.frame(x=myStrauss$x,y=myStrauss$y,v1I,v2I)

# Cluster:
myThomas = rThomas(50, 0.035, 8)
v1C=rnorm(length(myThomas$x), mean = 20, sd = 1)
v2C=rnorm(length(myThomas$x), mean = 0, sd = 5)
Cluster=data.frame(x=myThomas$x,y=myThomas$y,v1C,v2C)

# Iregular región:
#  Regular:
myRegular_cont <- rpoispp(450, win=polyowin)
v1R_cont=rnorm(length(myRegular_cont$x), mean = 20, sd = 1)
v2R_cont=rnorm(length(myRegular_cont$x), mean = 0, sd = 5)
Regular_cont=data.frame(x=myRegular_cont$x,y=myRegular_cont$y,v1R_cont,v2R_cont)

# Cluster:
myThomas_cont = rThomas(50, 0.03, 8,win=polyowin)v1C_cont=rnorm(length(myThomas_cont$x), mean = 20, sd = 1)
v2C_cont=rnorm(length(myThomas_cont$x), mean = 0, sd = 5)
Cluster_cont=data.frame(x=myThomas_cont$x,y=myThomas_cont$y,v1C_cont,v2C_cont)

# Inhibition:
 myStrauss_cont <- rStrauss(1000,0.7,0.05,W=polyowin)
 v1I_cont=rnorm(length(myStrauss_cont$x), mean = 20, sd = 1)
 v2I_cont=rnorm(length(myStrauss_cont$x), mean = 0, sd = 5)
Inhibition_cont=data.frame(x=myStrauss_cont$x,y=myStrauss_cont$y,v1I_cont,v2I_cont)
```

B) Descriptive, Histogram and Cumulative

```
par(mfrow=c(2,2))
ggplot(lgcp_irregular, aes(x = lgcp_irregular$v1R)) + geom_histogram(binwidth = 1)
ggplot(lgcp_irregular, aes(x = lgcp_irregular$v2R)) + geom_histogram(binwidth = 1)
ggplot(lgcp_irregular, aes(x = lgcp_irregular$v1R)) + geom_density()
ggplot(lgcp_irregular, aes(x = lgcp_irregular$v2R)) + geom_density()

Loc <- cbind(locR[,1], locR[,2])
head(Loc)
D <- dist(Loc)
par(mfrow = c(1,2), mar = c(5,5,2,2), cex.lab = 1.5)
hist(D, freq = TRUE, main = "", xlab = "Distance between sites",ylab = "Frequency")
text(0.08, 10000, "A", cex = 1.5)
plot(x = sort(D), y = (1:length(D))/length(D),
   type = "l",xlab = "Distance between sites",ylab = "Cumulative proportion")
text(0.2, 0.9, "B", cex = 1.5)
```

C) Mesh

```
S <- cbind(myRegular$x, myRegular$y)
locR=S
```

```
meshR <- inla.mesh.2d(locR, max.edge=c(100),cutoff=0.001)
plot(meshR)
points(locR, col = 1, pch = 16 , cex = 1)
meshR$n
meshR$loc[,1:2]
points(meshR$loc[,1:2])

# 9 meshes:
mesh1 <- inla.mesh.2d(Loc, max.edge=c(100, 100), cutoff = 0)
mesh2 <- inla.mesh.2d(Loc, max.edge=c(100, 100), cutoff = 0.1)
mesh3 <- inla.mesh.2d(Loc, max.edge=c(100, 100), cutoff = 0.01)
mesh4 <- inla.mesh.2d(Loc, max.edge=c(100, 100), cutoff = 0.001,offset=c(0,-0.2))
mesh5 <- inla.mesh.2d(Loc, max.edge=c(12500, 15000))
mesh6 <- inla.mesh.2d(Loc, max.edge=c(100, 100), cutoff = 0.25)
mesh7 <- inla.mesh.2d(Loc, max.edge=c(100, 100), cutoff = 0.15)
mesh8 <- inla.mesh.2d(Loc, max.edge=c(15, 15), cutoff = 0)
hull <- inla.nonconvex.hull(Loc)
mesh9 <- inla.mesh.2d(boundary = hull, max.edge=100, cutoff = 0)
#Number of vertices:
c(mesh1$n, mesh2$n, mesh3$n, mesh4$n, mesh5$n, mesh6$n,
  mesh7$n, mesh8$n, mesh9$n)

# Following 4 meshes:
bound1 <- inla.nonconvex.hull(Loc)
bound2 <- inla.nonconvex.hull(Loc, convex=0.3, concave=-0.15)
bound3 <- inla.nonconvex.hull(Loc, concave=0.5)
bound4 <- inla.nonconvex.hull(Loc, concave=0.1, resolution=c(300, 300))
mesh10 <- inla.mesh.2d(boundary = bound1, max.edge=100,  cutoff = 0)
mesh11 <- inla.mesh.2d(boundary = bound2, max.edge=100, cutoff = 0)
mesh12 <- inla.mesh.2d(boundary = bound3, max.edge=100, cutoff = 0)
mesh13 <- inla.mesh.2d(boundary = bound4, max.edge=100, cutoff = 0)
#Number of vertices: c(mesh10$n, mesh11$n, mesh12$n, mesh13$n)
```

D)   Models

#Regular case

```
S <- cbind(myRegular$x, myRegular$y)
locR=S
Loc <- cbind(locR[,1], locR[,2])
A1<- inla.spde.make.A(meshRegular, loc = Loc)
dim(A1)
spde_1  <- inla.spde2.matern(meshRegular, alpha = 2)
w.index <- inla.spde.make.index('w', n.spde = spde_1$n.spde)

Xm <- model.matrix(~ -1+Regular$v1R * Regular$v2R, data = Regular)
N <- nrow(Regular)
colnames(Xm)
X <- data.frame(V1        = Xm[,1], V2 = Xm[,2],V1.V2 = Xm[,3])

StackFit <- inla.stack(
 tag = "Fit",  data = list(y = X$V1),   A = list(1, 1, A1),
 effects = list( Intercept = rep(1, N), X = X, w = w.index))
```

 # Model1 (no spatial effect) and Model2 (spatial effect)
```
Model1 <- y ~ -1 + Intercept + V2 +V1.V2
Model2 <- y ~ -1 + Intercept + V2 +V1.V2 + f(w, model = spde_1)
IModel1 <- inla(Model1, family = "gaussian", data = inla.stack.data(StackFit),
        control.compute = list(dic = TRUE, waic = TRUE),
        control.predictor = list(A = inla.stack.A(StackFit)))
summary(IModel1)
IModel2 <- inla(Model2, family = "gaussian",
    data=inla.stack.data(StackFit), control.compute = list(dic = TRUE, waic = TRUE),
        control.predictor = list(A = inla.stack.A(StackFit)))
summary(IModel2)
# The same for all cases.
```

 # Model comparison (DIC, WAIC)

```
dic1  <- c(IModel1$dic$dic,IModel2$dic$dic,IModel3$dic$dic, IModel4$dic$dic,IModel5$dic$dic,IModel6$dic$di)
waic1 <- c(IModel1$waic$waic, IModel2$waic$waic,IModel3$waic$waic, IModel4$waic$waic,
IModel5$waic$waic,IModel6$waic$wai)
Z.out1     <- cbind(dic1, waic1)
rownames(Z.out1) <- c("Gaussian lm","","",
            "Gaussian lm + SPDE","","")
Z.out1
```

```
# Visualize the differences
Combined <- rbind(IModel1$summary.fixed[, c("mean", "0.025quant","0.975quant")],IModel2$summary.fixed[, c("mean",
"0.025quant", "0.975quant")])
Combined$WhichModel <- rep(c("lm", "spatial lm"), each = 3)
Combined$WhichVariable <- rep(rownames(IModel1$summary.fixed), 2)
colnames(Combined) <- c("Mean", "Lo", "Up", "WhichModel", "WhichVariable")
Combined

# Graphically

p <- ggplot()
p <- p + geom_point(data = Combined, aes(x = WhichModel, y = Mean))
p <- p + geom_errorbar(data = Combined, aes(x = WhichModel, ymax = Up,
                ymin = Lo), width=0.2)
p <- p + geom_hline(yintercept = 0, linetype = 2)
p <- p + xlab("Parameters") + ylab("Values")
p <- p + theme(text = element_text(size=15))
p <- p + facet_wrap( ~ WhichVariable, scales = "free_y")
p <- p + theme(legend.position="none")
p

# Hyperparameters
SpFi.w <- inla.spde2.result(inla = IModel1, name = "w",spde = spde_1,
                do.transfer = TRUE)
names(SpFi.w)
Kappa <- inla.emarginal(function(x) x, SpFi.w$marginals.kappa[[1]] )
sigmau <- inla.emarginal(function(x) sqrt(x),
                SpFi.w$marginals.variance.nominal[[1]] )
r <- inla.emarginal(function(x) x, SpFi.w$marginals.range.nominal[[1]] )
Kappa # POSTERIOR MEAN OF KAPPA
sigmau # POSTERIOR MEAN OF SIGMA U
r     # RANGE

# Correlation structure with the previous parameters
D      <- as.matrix(dist(meshRegular$loc[,1:2]))
d.vec <- seq(0, max(D), length = 100)
Cor.M <- (Kappa * d.vec) * besselK(Kappa * d.vec, 1)
Cor.M[1] <- 1
par(mfrow=c(1,1), mar = c(5,5,2,2))
plot(x = d.vec, y = Cor.M, pch = 16, type = "l", cex.lab = 1.5, xlab = "Distance",
    ylab = "Correlation", xlim = c(0, 0.3))
```

E)   Spatial random field
```
w.pm <- IModelo1b$summary.random$w$mean
w.proj <- inla.mesh.projector(meshRegular)
w.pm100_100 <- inla.mesh.project(w.proj, w.pm)
grid <- expand.grid(x = w.proj$x, y = w.proj$y)
grid$z <- as.vector(w.pm100_100)
levelplot(z ~ x * y, data = grid, aspect = "iso",
        scales = list(draw = TRUE),
        xlab = list("Easting ", cex = 1.5),
        ylab = list("Northing", cex = 1.5),
        main = list("Posterior mean spatial random field", cex = 1.5),
        panel=function(...){panel.levelplot(...)
          grid.points(x = Regular$x,
                y = Regular$y, pch = 1, size = unit(0.5, "char"))}  )
```

F)   The previous plot but in 3D
```
xygrid <- expand.grid(w.proj$x, w.proj$y)
Data3D <- data.frame(x = xygrid[,1],
                y = xygrid[,2],
                z = melt(w.pm100_100)[,3])
names(Data3D) <- c("x", "y", "z")
p <- ggplot(Data3D, aes(x, y, z = z), col = rgb(1, 0.5, 0.5, 0.7))
p <- p + stat_contour(geom="polygon",aes(fill = ..level..))
p <- p + geom_tile(aes(fill = z))
p <- p + stat_contour(geom="polygon",aes(fill = ..level..))
p <- p + stat_contour(aes(colour = ..level..))
p <- p + xlab("X") + ylab("Y")
p
```

G)   Model and standard deviation
```
grid.arrange(levelplot(inla.mesh.project(proj, field=IModel2$summary.fitted.values$mean[1:meshRegular$n]),
        xlab='X', ylab='Y ', scale=list(draw=TRUE), col.regions=topo.colors(30)),
```

```r
        levelplot(inla.mesh.project(proj, field=IModel2$summary.fitted.values$sd[1:meshRegular$n]),
              xlab='X', ylab='Y ', scale=list(draw=TRUE),
              col.regions=topo.colors(30)), nrow=1
```

H)   Model validation

```r
StackFit <- inla.stack(tag = "Fit",
 data = list(y = X$V1), A = list(1, 1, A1),
 effects = list(Intercept = rep(1, N), X = X, w = w.index))
IModel2_b <- inla(Model2,
          family = "gaussian",
          data=inla.stack.data(StackFit),
          control.compute = list(dic = TRUE, waic = TRUE),
          control.predictor = list(A = inla.stack.A(StackFit)))
FitIndex <- inla.stack.index(StackFit, tag = "Fit")$data
IModel1b.a <- IModel1b_b$summary.fitted.values[FitIndex,"mean"]
IModel1b.E <- X$V1 - IModel1b.a
plot(x = IModelo1b.a, y = IModelo1b.E)
plot(x = IModelo1b.a,  y = X$V1)
cor(IModelo1b.a, X$V1)
```

I)   Model interpretation

```r
Out.IModel1b <- IModel2_b$summary.fixed
print(Out.IModel1b, digits = 2)
#To get sigma for the equation
tau <- IModelo1b_b$marginals.hyperpar$`Precision for the Gaussian observations`
sigma <- inla.emarginal(function(x) (1/sqrt(x)), tau)
mean(tau)
sigma
```

J)   Prediction

```r
StackFit <- inla.stack(tag = "Fit",data = list(y = X$V1),
 A = list(1, 1, A1),  effects = list(
Intercept = rep(1, N), X = X, w = w.index))
dim(A1)
rowSums(A1)
colSums(A1)
dim(inla.stack.A(StackFit)) # 410 821
Xm <- model.matrix(~ -1+Regular$v1R * Regular$v2R, data = Regular)
X <- data.frame(V1      = Xm[,1],
          V2      = Xm[,2],
          V1.V2     = Xm[,3])
StackPred <- inla.stack(
 tag = "Predict",data = list(y = NA),A = list(1, 1),
 effects = list(Intercept = rep(1, nrow(X)), X = X))
dim(inla.stack.A(StackPred))
All.stacks=inla.stack(StackFit,StackPred)
dim(inla.stack.A(All.stacks))

IModel1b.pred <- inla(Model2b,
          family = "gaussian",
          data=inla.stack.data(All.stacks),
          control.compute = list(dic = TRUE),
          control.predictor = list(A = inla.stack.A(All.stacks)))

dim(IModel1b.pred$summary.fitted.values)
index.Fit <- inla.stack.index(All.stacks, tag = "Fit")$data
index.Pred <- inla.stack.index(All.stacks, tag = "Predict")$data

IModel1b.values <- IModel1b.pred$summary.fitted.values[index.Fit, c(1,3,5)]
IModel1b.pred <- IModel1b.pred$summary.fitted.values[index.Pred, c(1,3,5)]
dim(IModelo1b.values)
dim(IModelo1b.pred)

Dif=IModel1b.values[,1]-IModel1b.pred[,1]
plot(Dif1,ylim=c(-0.03,0.03))
abline(h=0.0)
```

K)   Simulation

```r
IModel1b.sim <- inla(Model1b, family = "gaussian", data=inla.stack.data(All.stacks), control.compute = list(config=TRUE),
control.predictor = list(A = inla.stack.A(All.stacks)))
set.seed(12345)
```

```
Simulation1=inla.posterior.sample(n=1,result=IModel1b.sim,seed=12345)
# Simulated data:
Simulation1[[1]]$latent
proj <- inla.mesh.projector(meshRegular)
meshRegular$n
levelplot(inla.mesh.project(proj, field=Simulation1[[1]]$latent[1:meshRegular$n]),
        xlab='X', ylab='Y ', scale=list(draw=TRUE), col.regions=topo.colors(30)
```
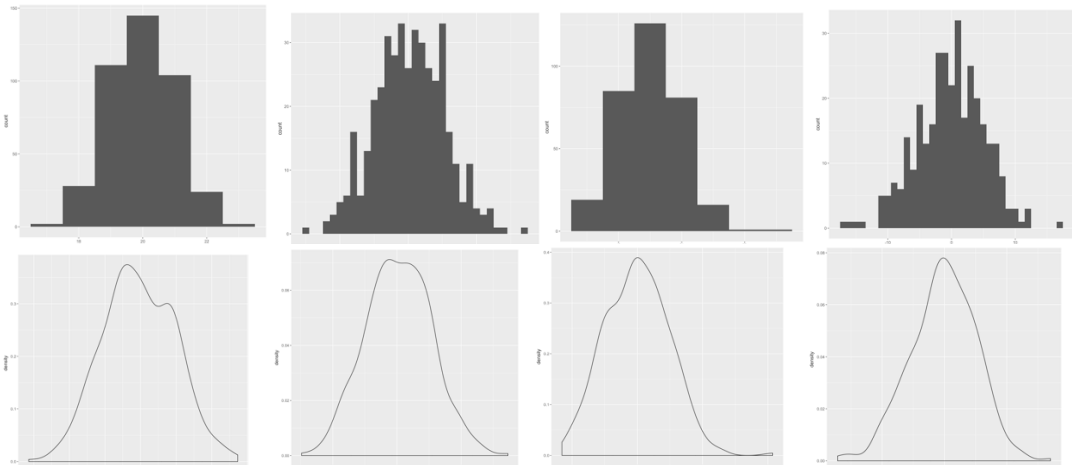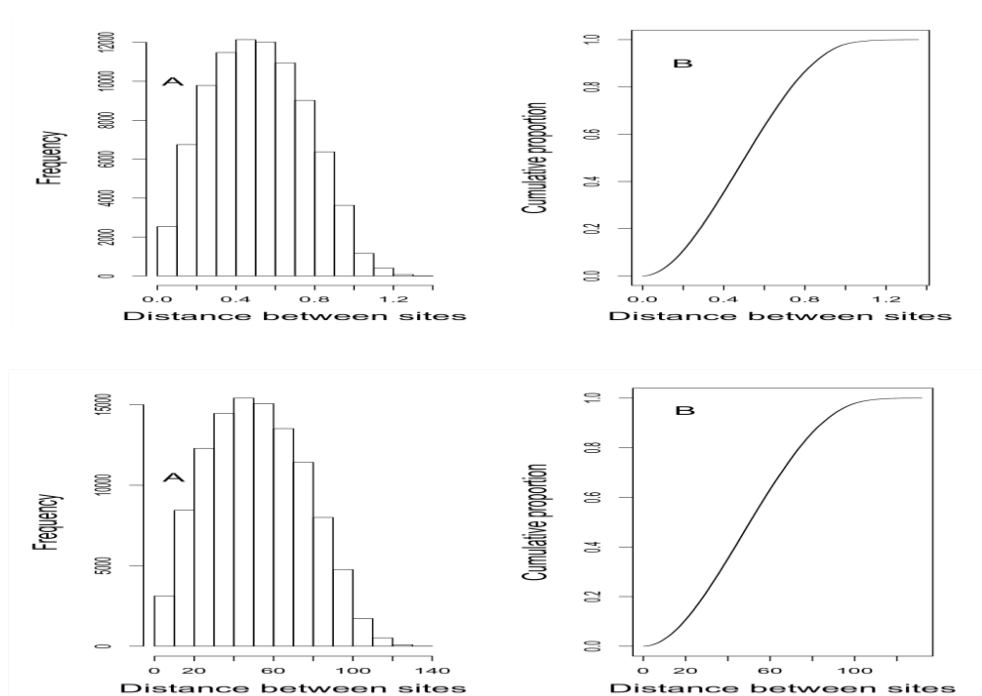
Appendix B: OTHER GRAPHICAL RESULTS

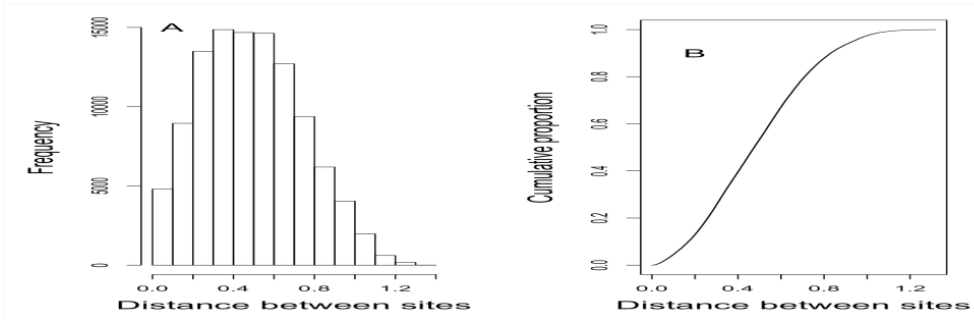Figure B1: Histogram (first row) and Density (second row) for the two variables in regular and irregular region (first row).

Figure B2: From first row to the last, Regular, Cluster and Inhibition, in regular regions.
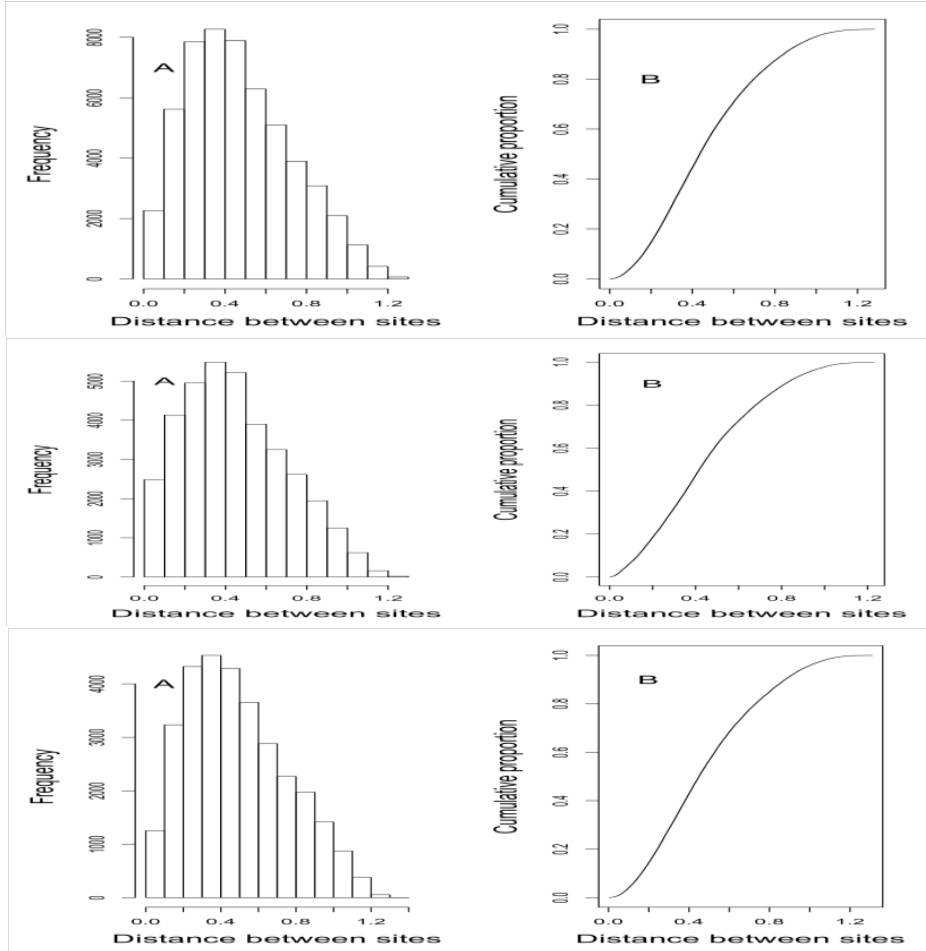
Figure B3: From first row to the last, Regular, Cluster and Inhibition, in irregular regions.
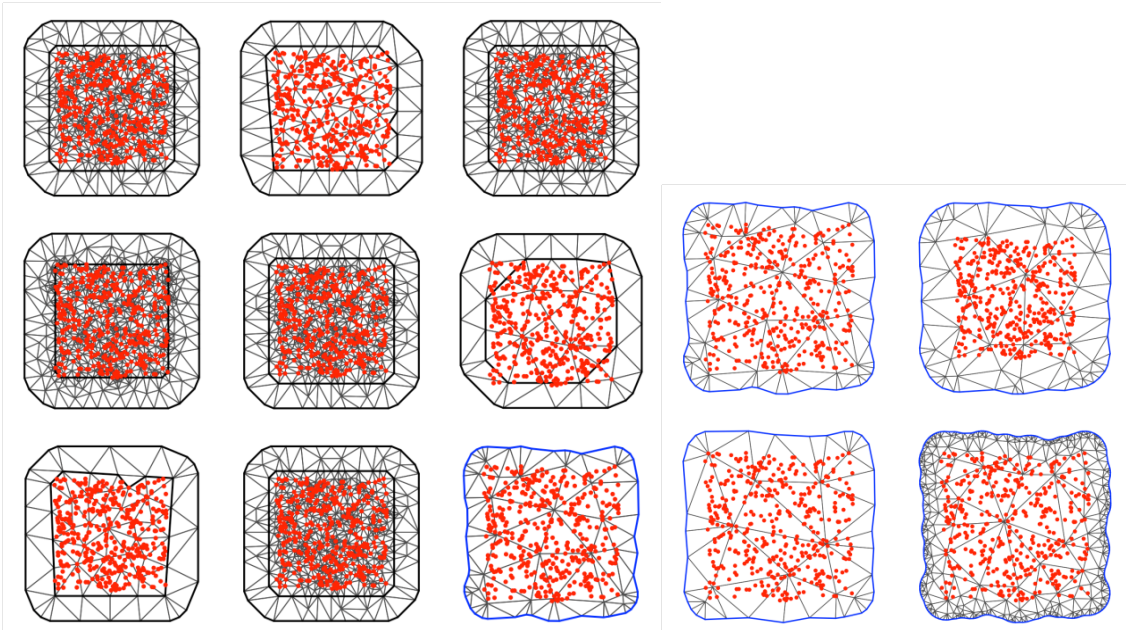
Figure B4: Regular data with a regular region. The 9 meshes on the left are presented without a non-convex function.
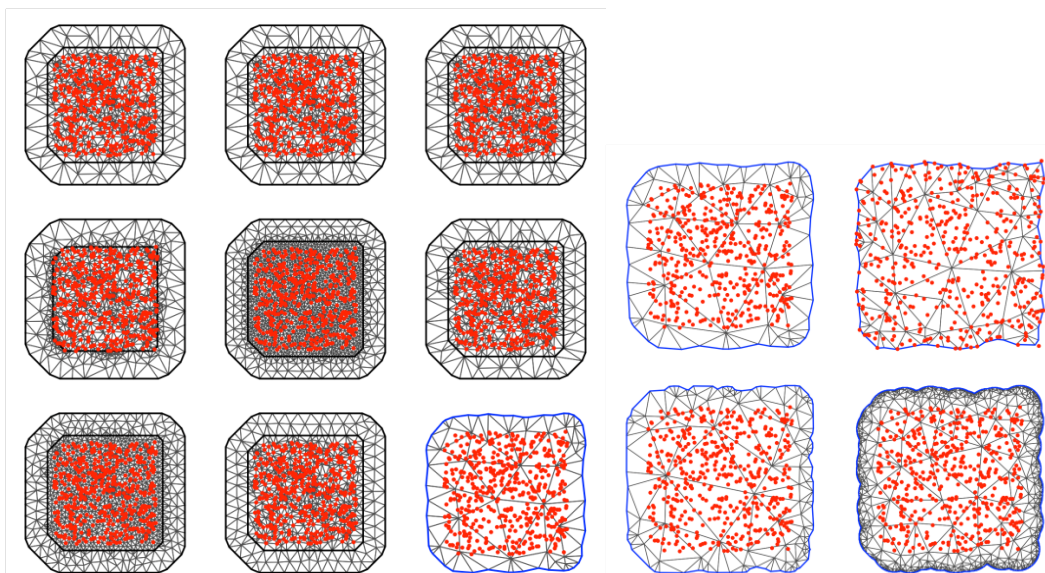
Figure B5: Inhibition data with a regular region. The 9 meshes on the left are presented without a non-convex function.
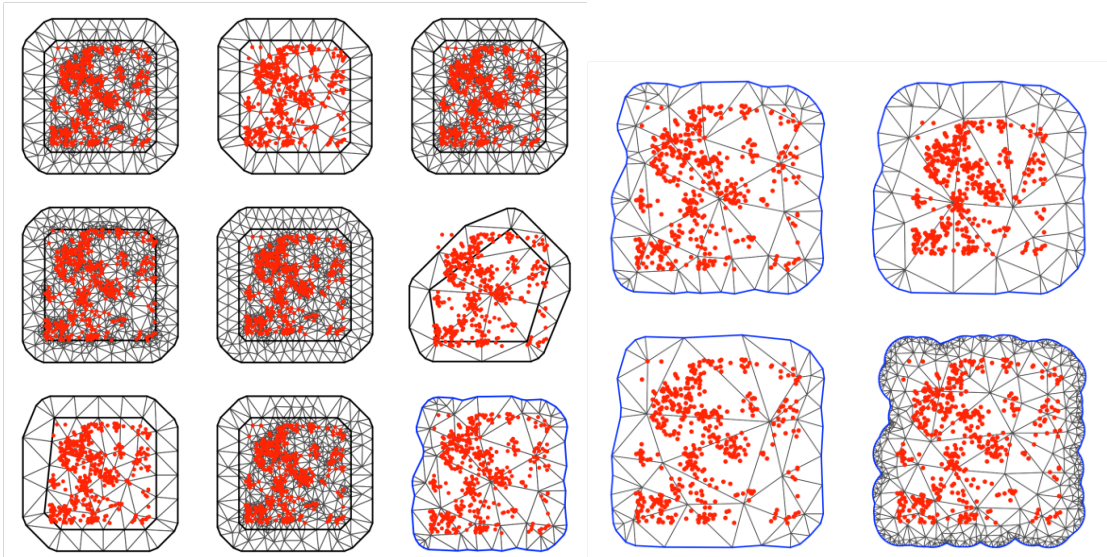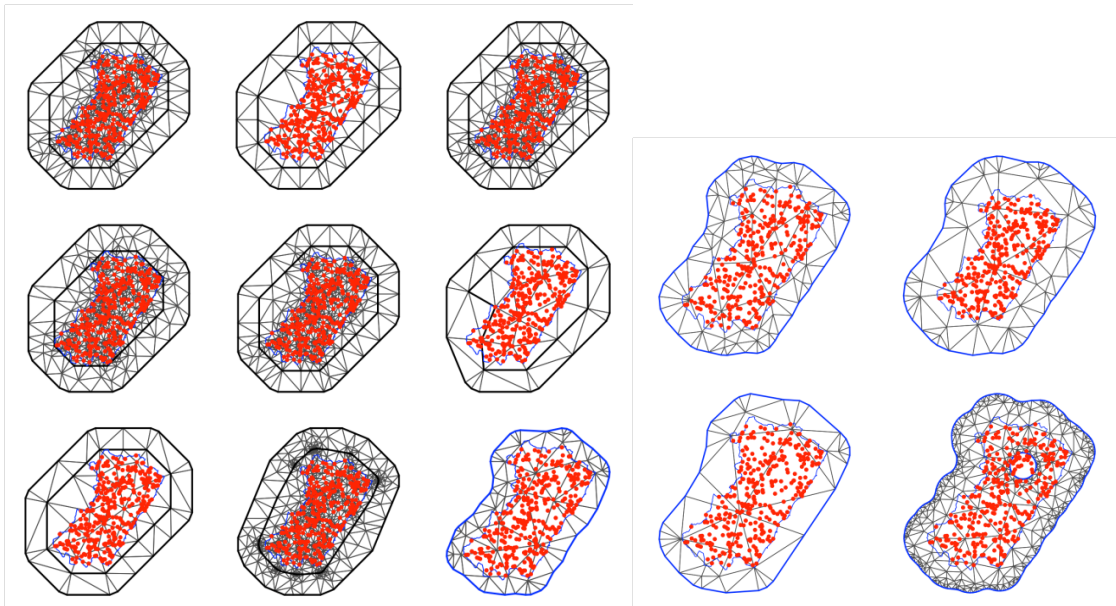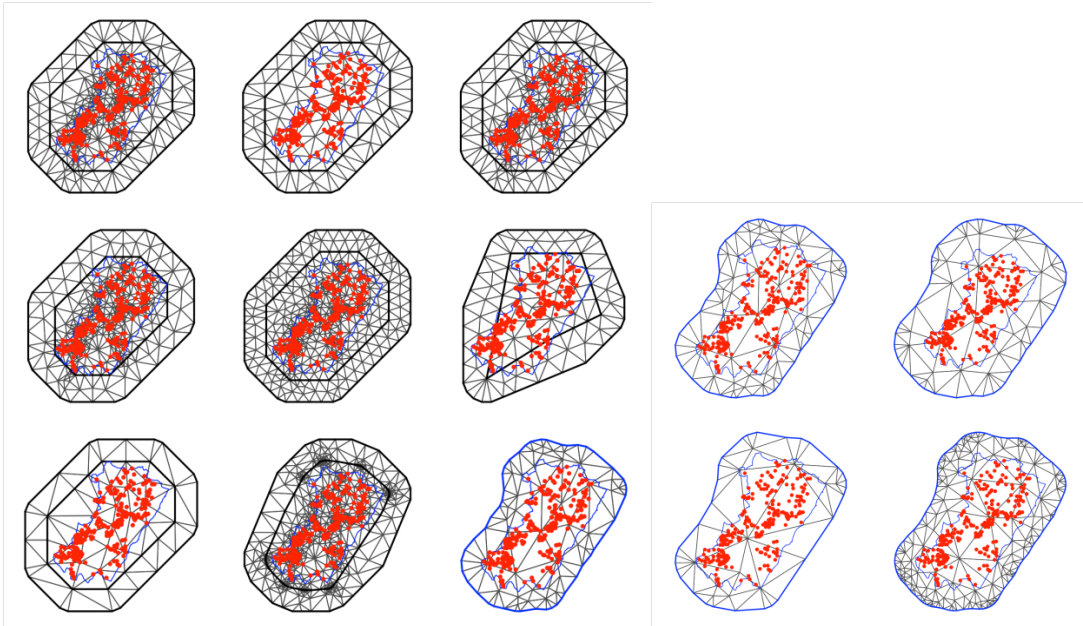
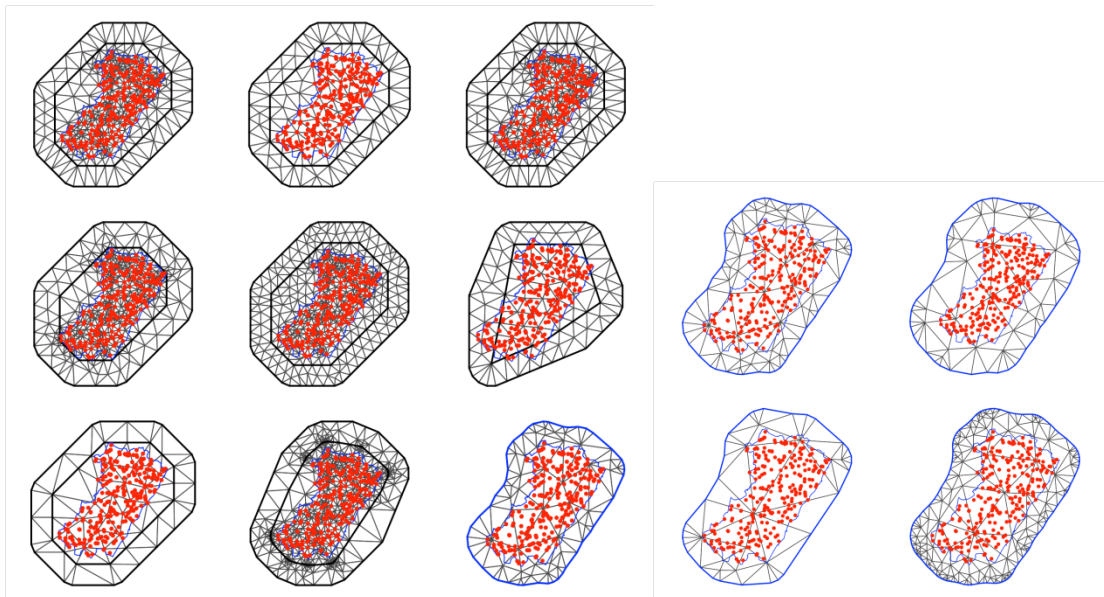Figure B6: Cluster data with a regular region. The 9 meshes on the left are presented without a non-convex function.

Figure B7: Regular data with an irregular region. The 9 meshes on the left are presented without a non-convex function.

Figure B8: Cluster data with an irregular region. The 9 meshes on the left are presented without a non-convex function.

Figure B9: Inhibition data with an irregular region. The 9 meshes on the left are presented without a non-convex function.
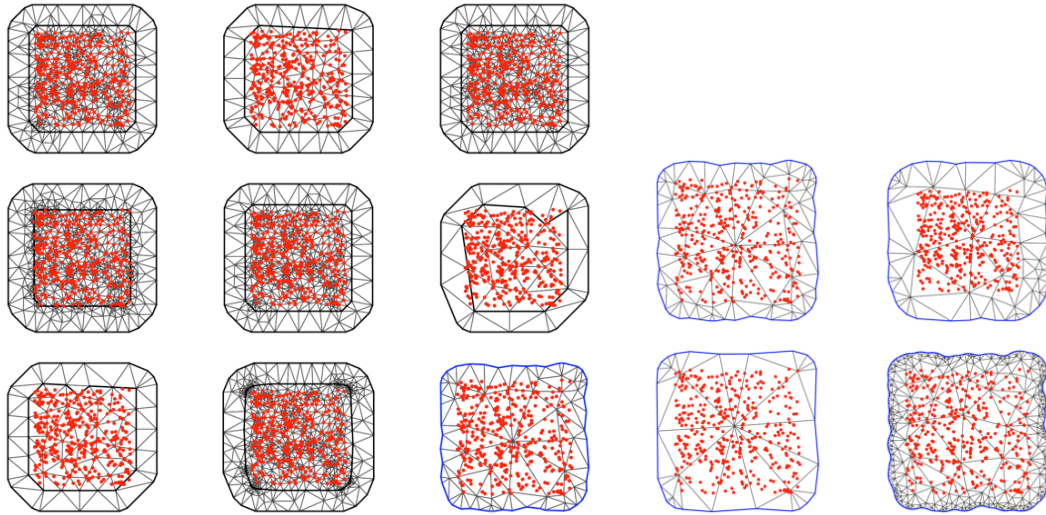
Figure B10: *Lgcp* data simulated in regular region and irregular region.
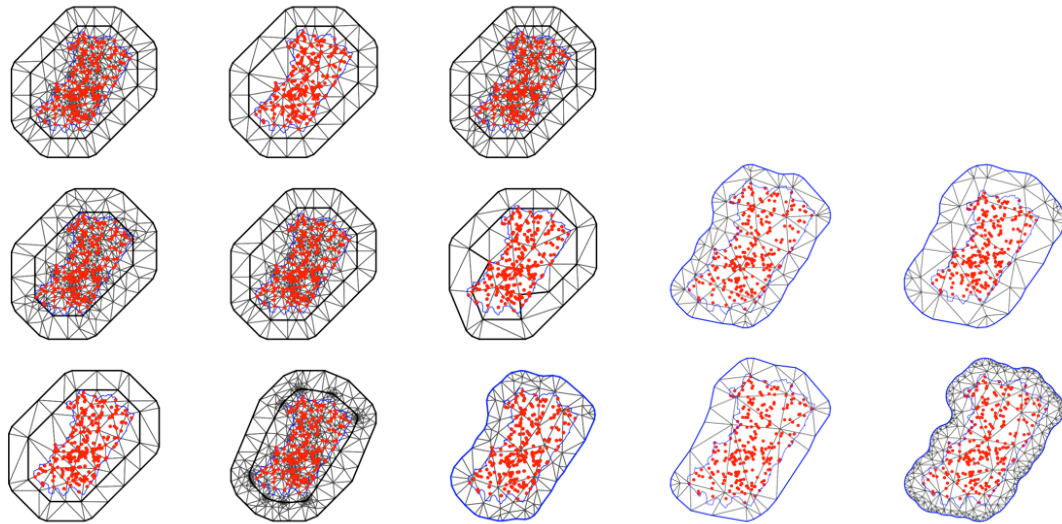

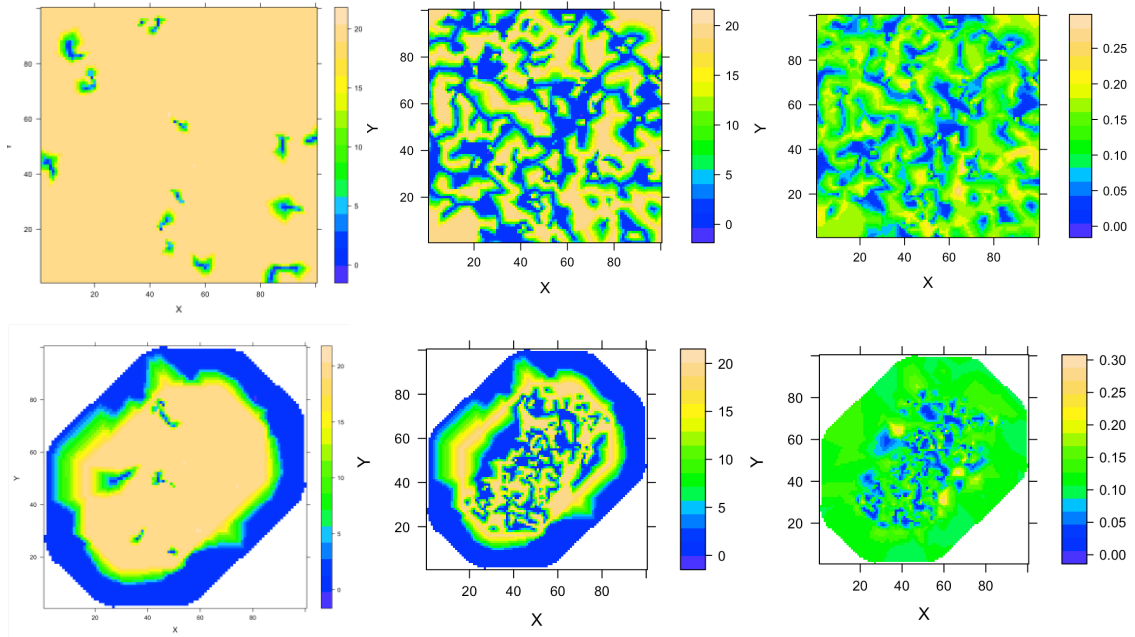Figure B11: *Lgcp* data simulated in irregular region and irregular region.

Figure B12: First row: Regular region, and second row: irregular region.
Simulated (left), Predicted (Center) and Standard Deviation (right).